Supporting Information

Sub-1.5 nm-Gapped Heterodimeric Plasmonic Nanomolecules

Xiaojun Song,[‡a] Yueliang Wang,[‡b] Yan Hao,[a] Qingqing Zhu,[a] Yanjuan Li,[a] Lei Song[a] and Zhaoxiang Deng*[a]

[a] Center for Bioanalytical Chemistry, Hefei National Research Center for Physical Sciences at the Microscale, Department of Chemistry, University of Science and Technology of China, Hefei, Anhui 230026, China. E-mail: zhxdeng@ustc.edu.cn

[b] College of Biological, Chemical Sciences and Engineering, Jiaxing University, Jiaxing, Zhejiang 314001, China

[‡] These authors contribute equally to this work.

Experimental Section

Chemicals. Chloroauric acid tetrahydrate ($HAuCl_4 \cdot 4H_2O$), chloroplatinic acid hexahydrate ($H_2PtCl_6 \cdot 6H_2O$), sodium sulfite (Na_2SO_3), citric acid monohydrate ($C_6H_8O_7 \cdot H_2O$), glycerol, $NaBH_4$, tetraethyl orthosilicate (TEOS), concentrated ammonia solution (28 wt%), and ethanol (99.7%) were purchased from Sinopharm Chemical Reagent Co., Ltd. (Shanghai, China). Bis(*p*-sulfonatophenyl) phenylphosphine dihydrate dipotassium salt (BSPP) and Sodium tetrachloropalladate (II) were products of Strem Chemicals (Newburyport, MA, USA). NaOH was bought from Sangon Bioengineering Technology and Services Co., Ltd. (Shanghai, China). Fish sperm DNA (FSDNA) and sodium citrate tribasic dihydrate were obtained from Sigma. $AgNO_3$, EDTA (Ethylene Diamine Tetraacetic Acid) disodium salt dehydrate, L-ascorbic acid, and NaCl were from Bio Basic Inc. (BBI, Canada). 4-Aminothiophenol (4-ATP) was bought from J&K Scientific (Beijing, China). Thiol-PEG_8-acid was purchased from Polypure AS (Oslo, Norway). All reagents were used as received without further purification.

DNA sequences. DNA oligonucleotides were custom-synthesized by Sangon Bioengineering Technology and Services Co., Ltd. (Shanghai, China) and purified by PAGE (unmodified DNA) or HPLC (thiolated DNA). All DNA oligos were subjected to molecular weight verification by MALDI-TOF mass spectroscopy. The sequences (5'-3') of the DNA oligonucleotides used in this work are listed as follows:

ssDNA (89 bases):
HS-5'GCAGTAACGCTATGTGACCGAGAAGGATTCGCATTTGTA***GTCTTGAGCCCGCACGAAACCTG GACACCCCTAAGCAACTCCGTATCAGA***3'

ssDNAc (89 bases):
HS-5'GCAGTAACGCTATGTGACCGAGAAGGATTCGCATTTGTA***TCTGATACGGAGTTGCTTAGGGG TGTCCAGGTTTCGTGCGGGCTCAAGAC***3'

(Note: underlined sequences in **ssDNA** and **ssDNAc** are complementary to each other and thus responsible for DNA-programmed nanoparticle assembly)

AuNPs. Gold nanoparticles with a diameter of 13 nm were synthesized by a citrate-based chemical reduction of chloroauric acid according to literature.[1] The as-obtained 13 nm AuNPs were then employed as nucleation seeds to grow larger AuNPs with diameters of 23 nm and 30 nm based on a published procedure.[2]

AgNPs. The synthesis of silver nanoparticles with a diameter of 28 nm followed a previously developed method with slight modification.[3] 30 mL glycerol was combined with 40 mL deionized H_2O in a 100 mL flask. The resulting mixture was heated up in an oil bath maintained at 106°C for 30 min. To the above solution was added 18 mg $AgNO_3$ dissolved in 1 mL H_2O under vigorous magnetic stirring. 1 min later, 2 mL sodium citrate (3%) solution was introduced to initiate a chemical reduction reaction. The reaction continued in the oil bath for 1 h under constant stirring, and then terminated by cooling down the solution to room temperature.

A**u-coated AgNPs (g-AgNPs).** The as-synthesized AgNPs was coated by a thin layer of gold to achieve

improved chemical and colloidal stabilities following an established procedure with slight modifications.[4] A growth solution for the Au shells was made with a typical recipe containing 4.81 mL of H_2O, 78 μL of 127 mM $HAuCl_4$, 50 μL of 1 M NaOH, and 60 μL of 0.5 M Na_2SO_3. Such a solution was aged for 12 h at room temperature without stirring prior to use. For the Au coating of AgNPs, 15 mL of the as-synthesized 30 nm AgNPs, 75 mL of 0.058 mg/mL FSDNA, 75 mL of 0.1 M L-AA, 11.25 mL of 1 M NaOH, and 5.25 mL of 0.1 M Na_2SO_3 were first combined in a 250 mL flask. Subsequently, 10 mL of the aged growth solution was added to this mixture. The sample was then incubated in a 45℃ oven overnight to accomplish the reaction. To obtain pinhole-free Au layers on the AgNPs, it was necessary to harvest the products by centrifugation, and repeat the coating procedure one more time. The above solution was concentrated into 4 mL by centrifugation, and combined with 20 mL of 0.58 mg/mL FSDNA, 20 mL of 0.1 M L-AA, 3 mL of 1 M NaOH, and 1.4 mL of 0.1 M Na_2SO_3 in a 50 mL flask. After a thorough mixing， 1 mL of the aged growth solution was introduced. The resulting mixture was incubated in a 45℃ oven overnight to obtain AgNPs with pinhole-free gold coating (g-AgNPs). The increased FSDNA concentration during the second gold plating was critical to minimize a thickness increase of the gold shells, which was nevertheless very effective for pinhole removal.

PtNPs. Suprastructured PtNPs with a diameter of 47 nm were synthesized via a stepwise seeded-growth process.[5] The synthesis started with 3-4 nm PtNPs as heterogeneous nucleation seeds for the growth of 29 nm PtSPs. The as-obtained 29 nm PtSPs were then used to seed the synthesis of 47 nm PtNPs. The 3-4 nm PtNP seeds were synthesized by $NaBH_4$ reduction of H_2PtCl_6 in the presence of citrate ligands. During the overgrowth of successively thicker Pt outer layers, L-AA was used as a reducing agent.

PdNPs. Pd nanoparticles with a diameter of 37 nm were synthesized through a successive seeded-growth started with 3-4 nm PdNPs. To obtain the 3-4 nm PdNP seeds,[6] 30 μL of 0.1 M sodium citrate was first combined with 1 mL of 1 mM Na_2PdCl_6 under magnetic stirring at room temperature, followed by introducing 10 μL of freshly prepared 100 mM sodium borohydride. The PdNP seeds with a diameter of 3-4 nm were obtained after a reaction for 10 min. The as-prepared PdNP seeds were used to grow 10 nm PdNPs. Briefly, to 30 mL of deionized water (pre-cooled in an ice-water bath) was sequentially added 400 uL of the seed solution, 20 uL Na_2PdCl_4 (0.4 mM), and 1 mL sodium critrate (100 mM); Subsequently, 6 mL of ice-cooled L-AA (50 mM) was introduced dropwise to the above solution under continuous stirring to initiate a seeded Pd growth. The reaction was allowed to continue for 50 min after the addition of L-AA. The resulting 10 nm PdNPs were then taken as secondary seeds for the growth of 37 nm PdNPs following a similar procedure addressed above.

BSPP ligand exchange. Bis(*p*-sulfonatophenyl)phenylphosphine dihydrate dipotassiumsalt (BSPP) was added to a nanoparticle solution to reach an appropriate concentration (0.5 mg/mL for AuNPs and g-AgNPs, 1 mg/mL for 47 nm PtNPs, and 0.75 mg/mL for 37 nm PdNPs) in order to accomplish a ligand exchange. The as-obtained BSPP-capped nanoparticles were collected by centrifugation, and re-dispersed in deionized water.

Minimally DNA-conjugated AuNPs, g-AgNPs, PtNPs, and PdNPs. Suitable amounts of 5'-thiolated ssDNA or ssDNAc were combined with the nanoparticles in a 0.5×TBE (Tris, 44.5 mM; EDTA, 1 mM; boric acid, 44.5 mM; pH 8.0) buffer supplemented with an appropriate concentration of NaCl. The DNA conjugation reaction took place during an overnight incubation at room temperature. The DNA-conjugated nanoparticles were

collected by centrifugation, and redispersed in 0.5×TBE. Such a centrifugation-redispersion cycle was repeated 3 times to remove unbound DNA stands.

DNA-directed nanodimer assembly. Nanoparticles minimally functionalized by complementary DNA strands were hybridized in a 0.5×TBE buffer containing a suitable amount of NaCl at room temperature for 10 h. 1.5% agarose gel electrophoresis was employed to analyze and isolate the assembled nanodimers.

EtOH-assisted Ag^+ soldering of DNA-bonded nanodimers. One volume of an aqueous solution of DNA-linked nanoparticle dimers was combined with nine volumes of ethanol to form pre-coupled nanostructures driven by ethanol-enhanced double layer neutralization.[7] The immediately coupled dimers were transferred to an Ag^+ soldering cocktail containing 2 μg/μL FSDNA and an appropriate amount of $AgNO_3$ for a quick fixation of the coupled dimers.[8] The fixated structures were stable in an aqueous solution without losing their in-ethanol coupling, allowing agarose gel electrophoretic and spectroscopic characterizations.

Silica coating. To 1.5 mL of an ethanol solution containing 0.15 mL of water was slowly added 25 μL of DNA-linked nanoparticle dimers. Afterwards, 30 μL of aqueous ammonia (28%) and 300 μL of tetraethyl orthosilicate (TEOS, 1% in ethanol) were sequentially introduced to the above solution under stirring.[9] After a reaction for 12 h, the silica-encapsulated dimers were collected by centrifugation at 6000 g for 5 min, and re-dispersed in H_2O. Multiple centrifugation-redispersion cycles were necessary to remove homogeneously nucleated SiO_2 nanoparticles from the products.

Spectroscopic and TEM characterizations: Extinction spectra were recorded on Hitachi U-2910 and Shimadzu UV3600 spectrophotometers. Transmission electron microscopy (TEM) images were taken on an HT7700 TEM facility operated at an electron acceleration voltage of 100 kV. Samples for TEM imaging were deposited on carbon-coated copper grids from their aqueous solution droplets. The samples were dried air upon removal of residual liquids by a piece of filter paper before TEM observation.

Electromagnetic simulations based on a boundary element method (BEM). We employed a Matlab Toolbox to carry out BEM-based plasmonic simulations.[10-12] The toolbox solves Maxwell's equations for a dielectric environment where homogeneous and isotropic dielectric functions are separated by abrupt boundaries. For systems that fall into this assumption, only the interfaces (not the whole volume) between different dielectric matters are discretized for computations. Accordingly, simulations based on a BEM method are very fast and memory efficient.

References:

[1] G. Frens, *Nat. Phys. Sci*., 1973, **241**, 20.

[2] N. G. Bastús, J. Comenge and V. Puntes, *Langmuir*, 2011, **27**, 11098.

[3] D. Steinigeweg and S. Schlücker, *Chem. Commun*., 2012, **48**, 8682.

[4] Z. Zhang, K. Bando, A. Taguchi, K. Mochizuki, K. Sato, H. Yasuda, K. Fujita and S. Kawata, *ACS Appl. Mater. Interfaces*, 2017, **9**, 44027.

[5] N. C. Bigall, T. Härtling, M. Klose, P. Simon, L. M. Eng and A. Eychmüller, *Nano Lett*., 2008, **8**, 4588.

[6] K. Naoe, C. Petit and M. P. Pileni, *Langmuir*, 2008, **24**, 2792.
[7] Y. Hao, L. Fang, and Z. Deng, *CCS Chem.*, 2020, **2**, 1359.
[8] Y. Wang, L. Fang, G. Chen, L. Song and Z. Deng, *Small*, 2018, **14**, 1703303.
[9] C. Graf, D. L. J. Vossen, A. Imhof and A. van Blaaderen, *Langmuir*, 2003, **19**, 6693.
[10] F. J. Garcia de Abajo and A. Howie, *Phys. Rev. B*, 2002, **65**, 115418.
[11] F. J. Garcia de Abajo, *Rev. Mod. Phys.*, 2010, **82**, 209.
[12] U. Hohenester and A. Trügler, *Comp. Phys. Commun.*, 2012, **183**, 370.

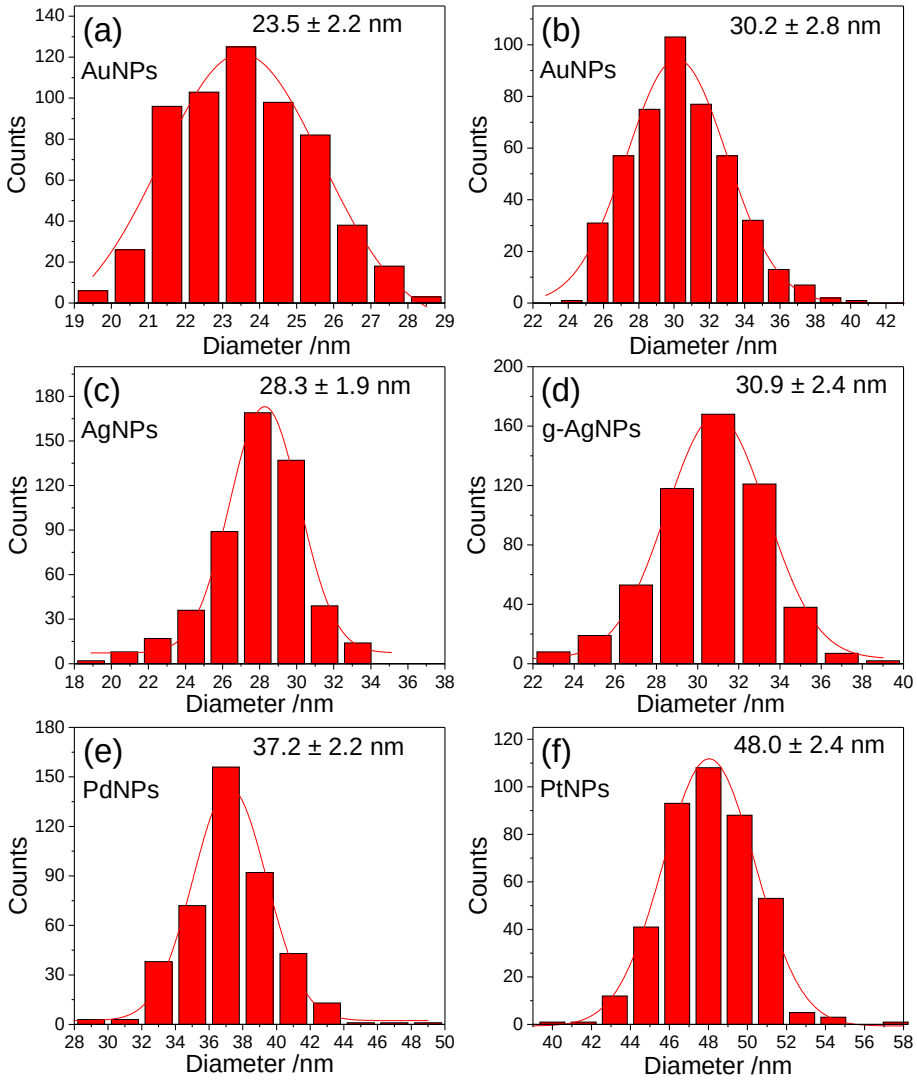

Figure S1. Statistical charts showing the size distributions of as-synthesized nanoparticles.

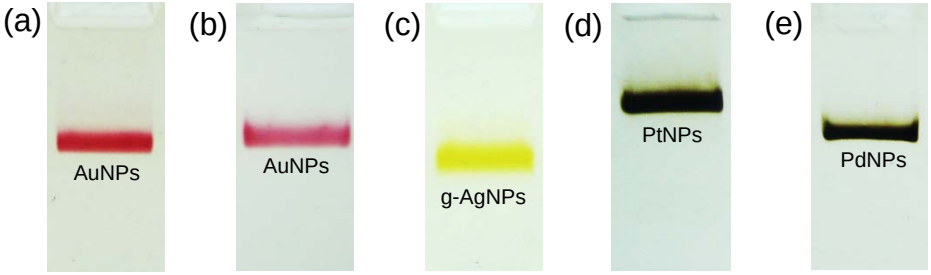

Figure S2. Agarose gel electropherograms of as-synthesized 23 (a) and 30 nm (b) AuNPs, 31 nm g-AgNPs (c), 48 nm PtNPs (d) and 37 nm PdNPs (e).

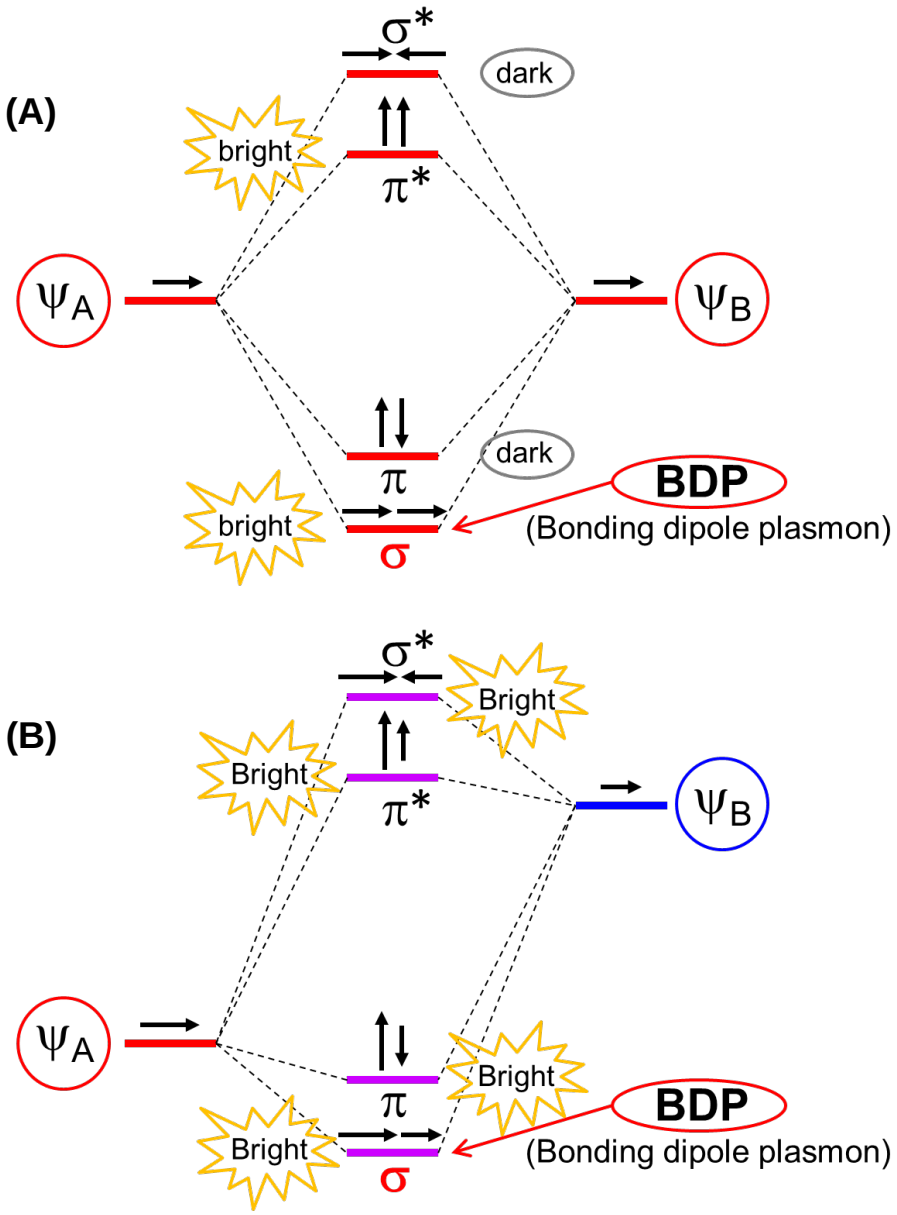

Figure S3. Hybridization models representative of longitudinal ("σ bonding") and transverse ("π bonding") dipolar plasmon couplings of a homodimer of identical nanoparticles (A) and a heterodimer comprising nanoparticles of different sizes or compositions (B). The lowest energy levels represent bonding dipole plasmons (BDPs) as a result of two closely positioned dipoles with a head-to-tail alignment. Interband continuum is omitted from the models for clarity, which however does have an influence on high energy LSPR modes and the profiles (damping-related peak broadening) of the BDPs especially for dimers containing PtNPs and PdNPs.

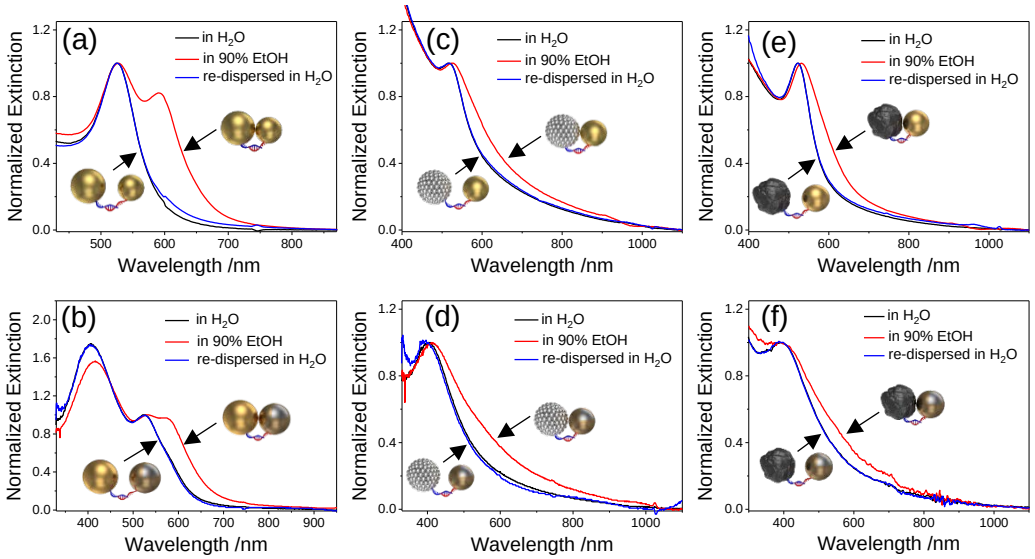

Figure S4. Extinction spectra of heterodimers in different solutions. Panels (a-f) correspond to dimers of various compositions including $Au_{30}Au_{23}$ (a), $Au_{30}Ag@Au_{31}$ (b), $Au_{30}Pt_{48}$ (c), $Ag@Au_{31}Pt_{48}$ (d), $Au_{30}Pd_{37}$ (e), and $Ag@Au_{31}Pd_{37}$ (f), respectively. *The dimers exhibit almost identical extinction profiles after in-ethanol coupling and being transferred back to water, further evidencing the coupling-induced spectral features.*

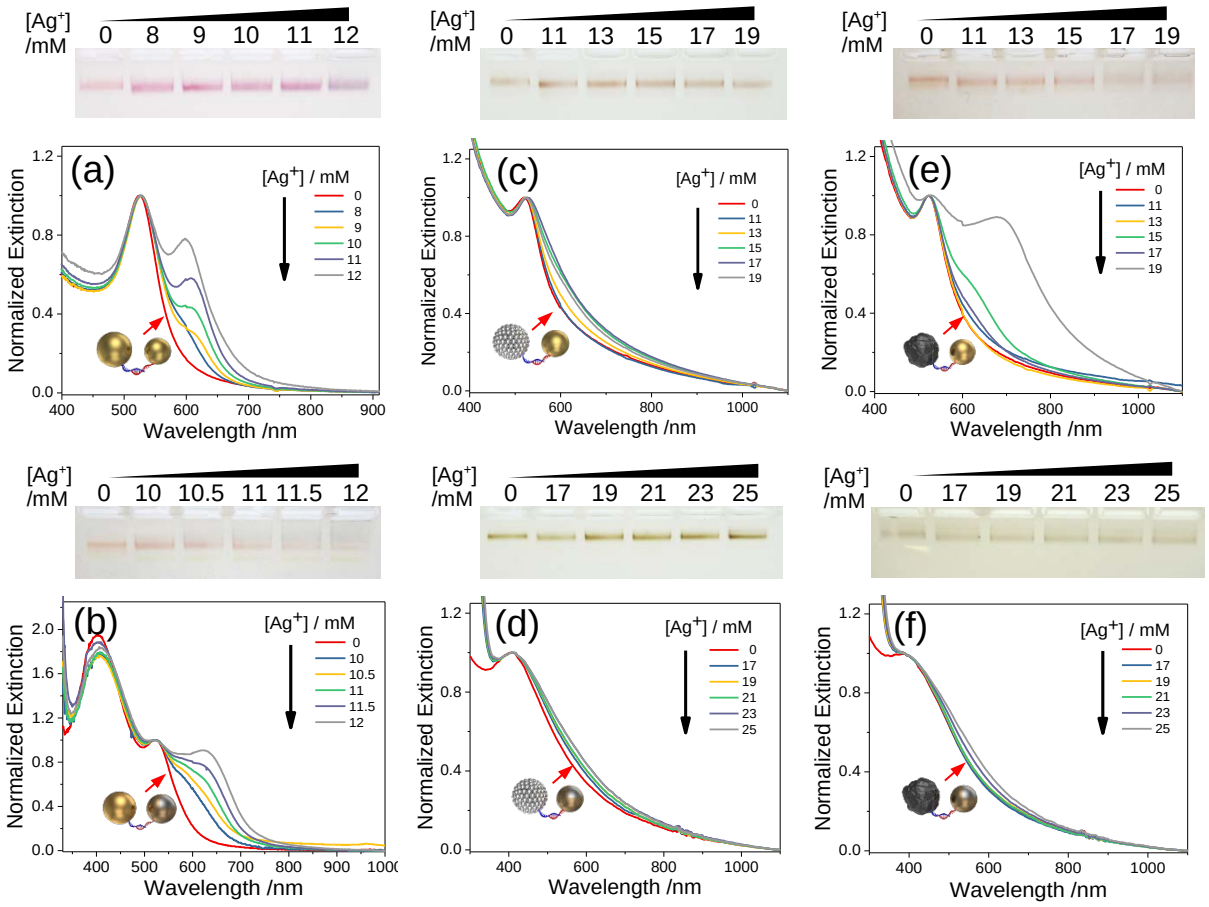

Figure S5. Optical extinction spectra and agarose gel electropherograms of AIS-treated, DNA-assembled heterodimers of various NP compositions including (a) $Au_{30}Au_{23}$, (b) $Au_{30}Ag@Au_{31}$, (c) $Au_{30}Pt_{48}$, (d) $Ag@Au_{31}Pt_{48}$, (e) $Au_{30}Pd_{37}$, and (f) $Ag@Au_{31}Pd_{37}$, respectively. *These data revealed that in some cases ((b) and (e)) aggregation happened for the samples directly treated by AIS (in the absence of in-ethanol pre-coupling) with increased Ag^+ concentrations before an optimal and stable coupling is achieved.*

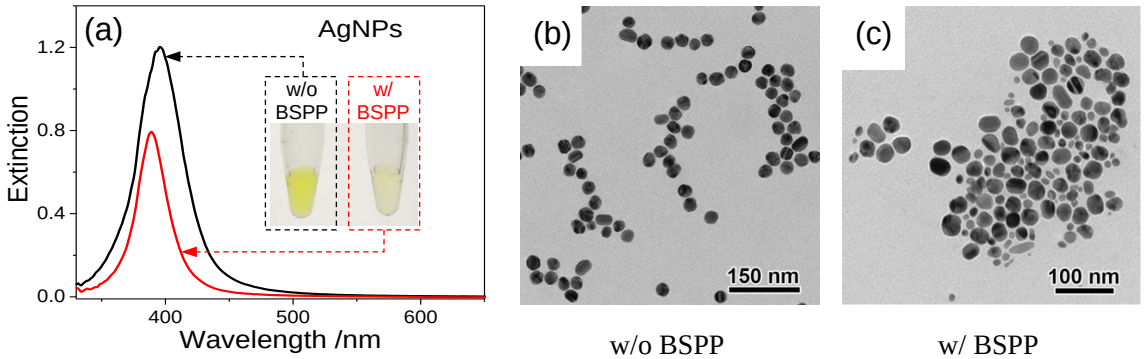

Figure S6. Oxidative leaching instability of AgNPs. (a) Optical extinctions of AgNPs with or without a BSPP (0.5 mg/mL) treatment for 2 hours. (b-c) TEM images of AgNPs before and after chemical leaching. *Note: BSPP forms a stable Ag^+ complex to accelerate an oxidative etching of AgNPs by dissolved oxygen. The smaller AgNPs in (c) could be partially etched products.*

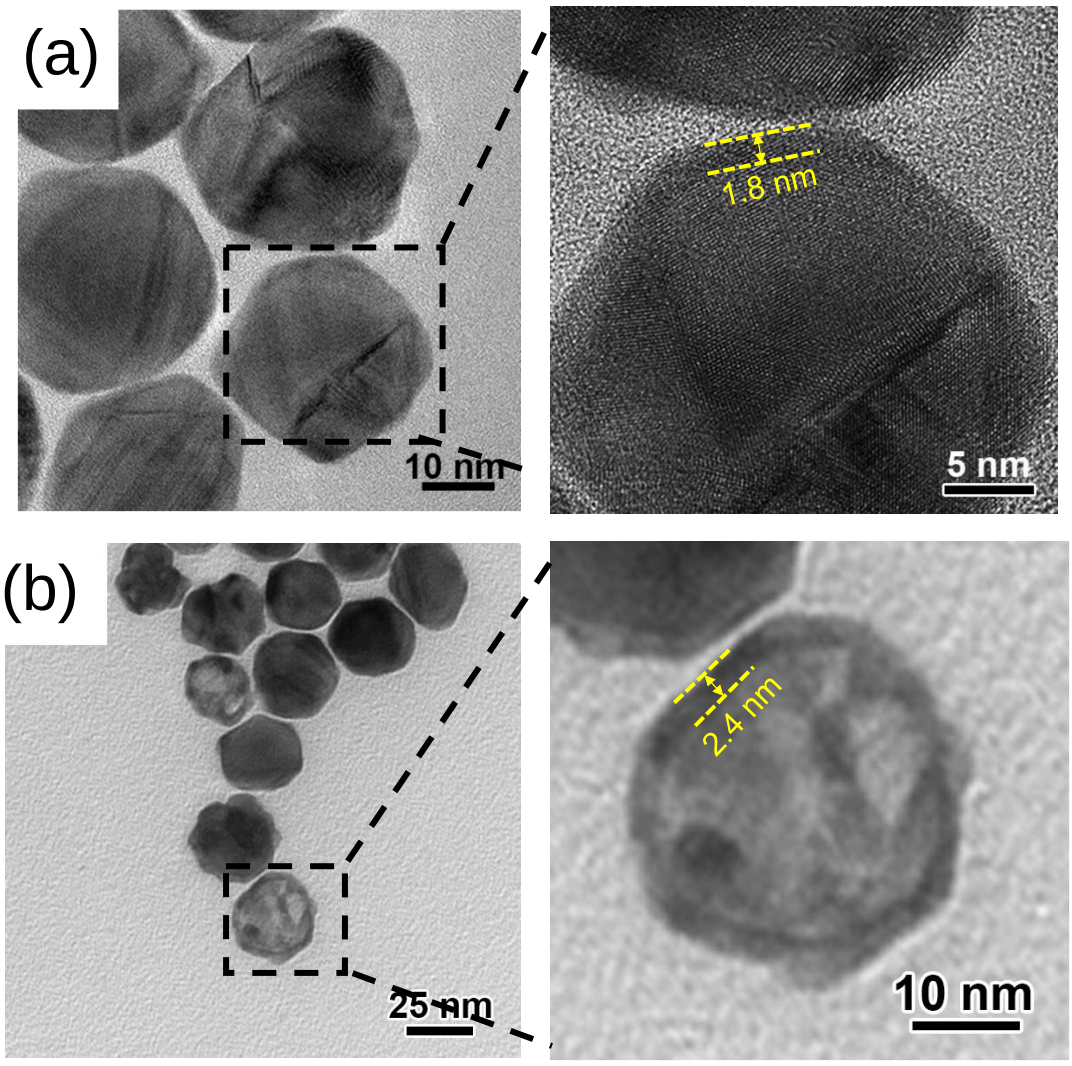

Figure S7-1. (a) High resolution TEM (HRTEM) imaging of gold shells grown on AgNPs after two times of gold plating operations. (b) Rarely found Au (strictly Au/Ag alloy) cages after a heavy H_2O_2 etching of the g-AgNPs in (a). *It is clear that the Au shells after the H_2O_2 etching became thickened due to a shrinkage of the cage structures upon silver removal.*

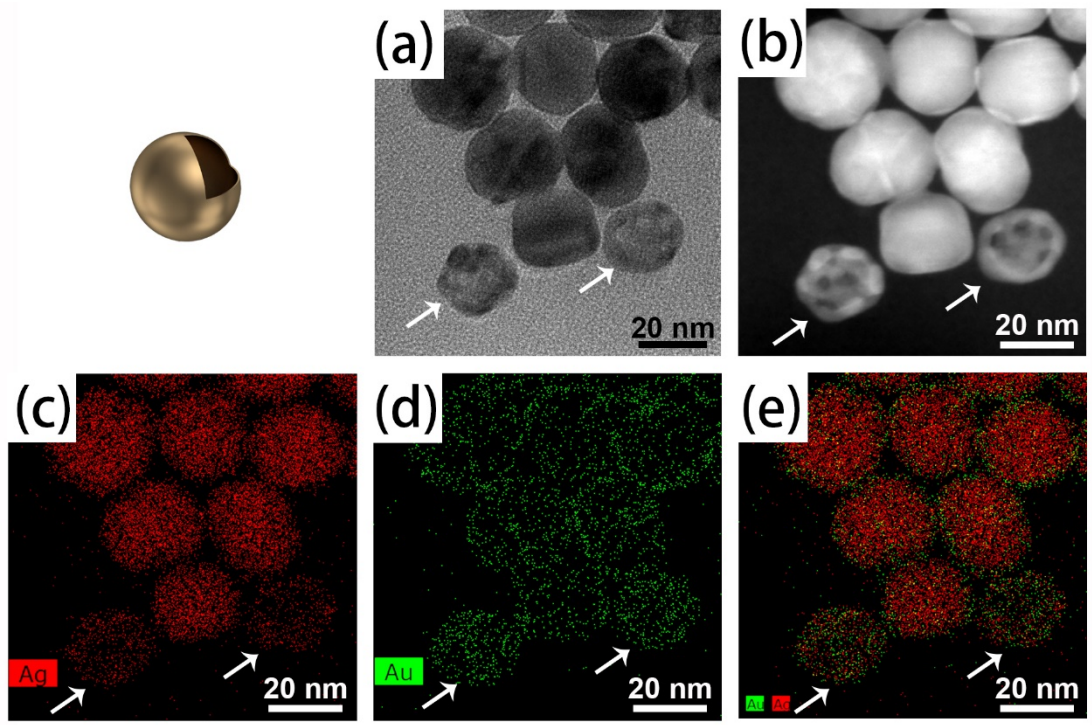

Figure S7-2. Bright- (a) and dark-field (b) TEM images and EDX element mapping (c-e) of as-synthesized g-AgNPs after a heavy H_2O_2 etching. Arrows indicate two rarely observed Au (strictly Au/Ag alloy) cages.

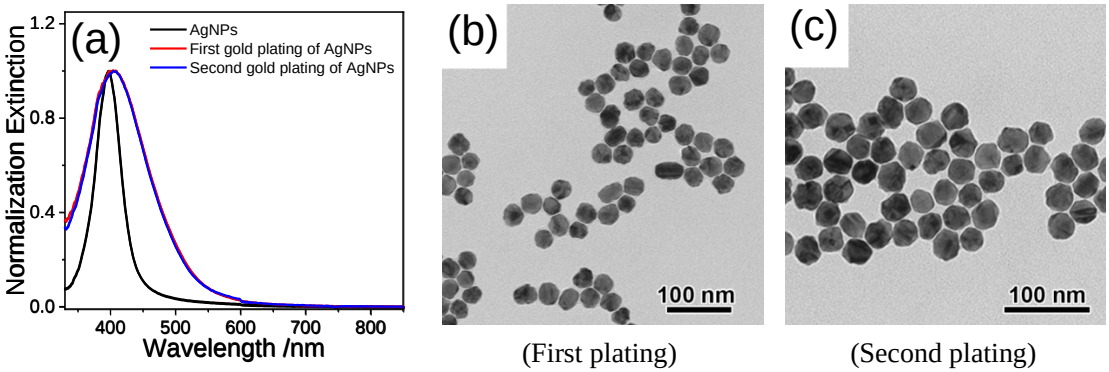

(First plating) (Second plating)

Figure S8. (a) Optical extinction profiles of AgNPs and corresponding gold-plated products. (b, c) TEM images of AgNPs after one (b) and two (c) gold platings.

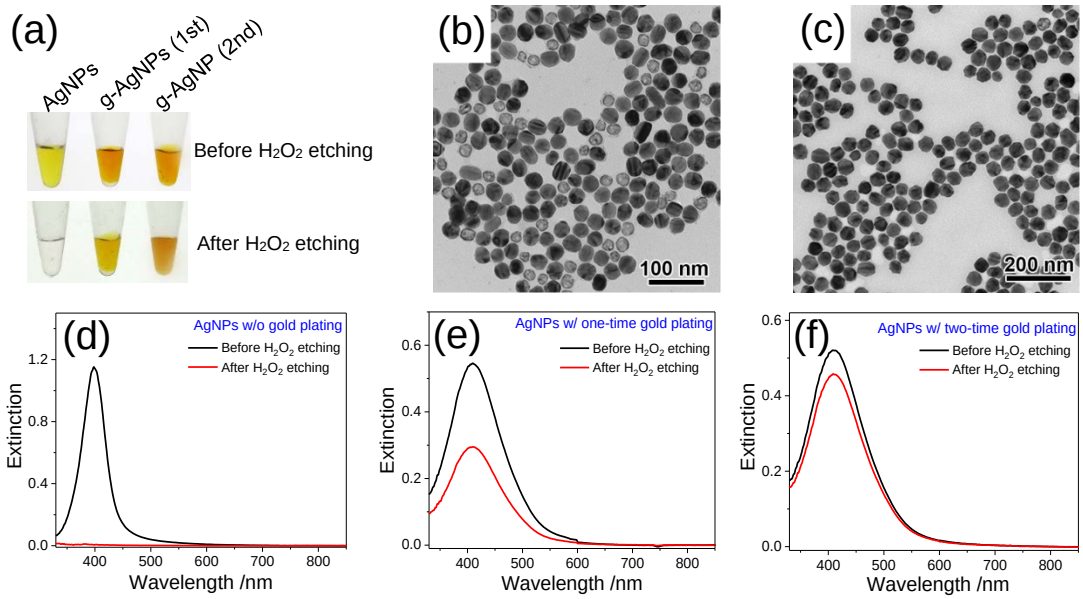

Figure S9. H_2O_2 etching tests of AgNPs and gold-plated AgNPs (g-AgNPs). (a) Photos of AgNPs and g-AuNPs before and after an etching by 0.8 M H_2O_2 for 24 hours. (b, c) TEM images of H_2O_2-etched g-AgNPs after the first (b) and second (c) gold plating operation. (d-f) UV-Vis spectra of AgNPs (d) and g-AgNPs (e, f) before and after H_2O_2 etching. *These data verified the enhanced oxidation-resistivity of AgNPs after gold plating. The second plating did not significantly alter the extinction profile (a reflection of gold shell thickness) of the NPs but greatly improved their stability probably due to reduced pin holes in the gold outer layers.*

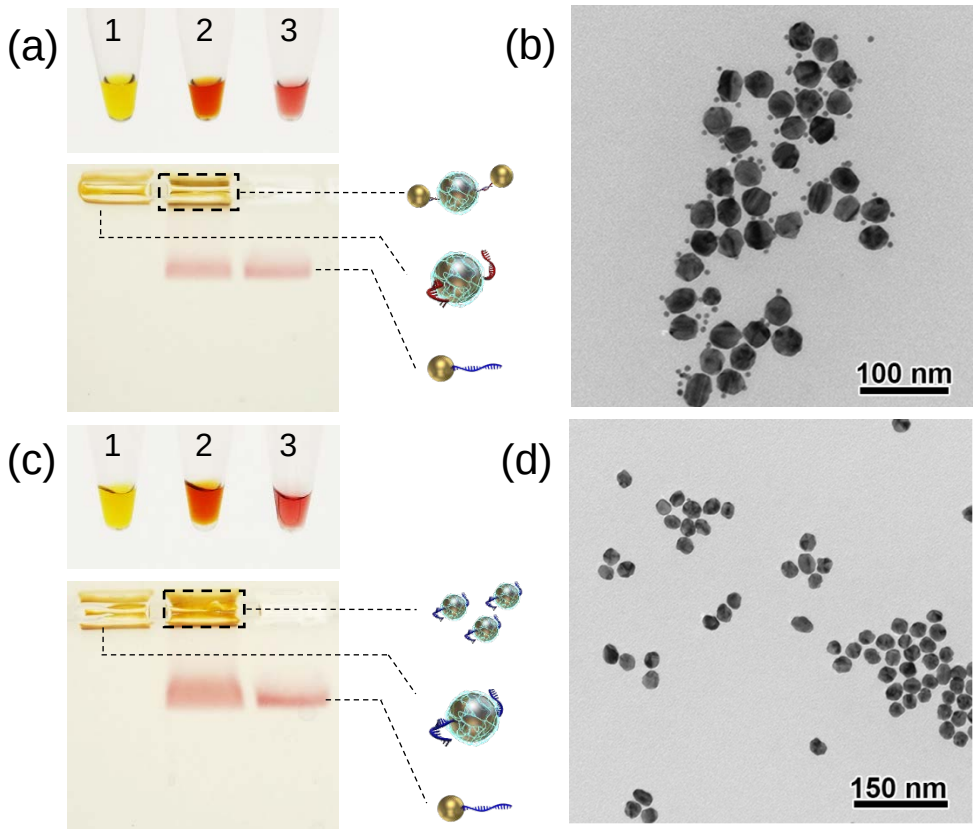

Figure S10-1. (a, b) Agarose gel electrophoresis and TEM imaging showing DNA-directed self-assembly between DNA-functionalized 31 nm g-AgNPs (PVP-capped) and 5 nm AuNPs. Samples 1 and 3 in (a) depict PVP-capped g-AgNPs with minimal ssDNA decoration and BSPP-capped 5 nm AuNPs monofunctionalized by ssDNAc, respectively. Sample 2 is a hybridization mixture between samples 1 and 3. The assembled product is trapped in the gel and imaged by TEM (b). (c, d) A control experiment by replacing the ssDNA functionality with ssDNAc for PVP-capped g-AgNPs. As a result, the g-AgNPs recovered from the gel well did not capture any 5 nm AuNPs (d) due to the non-complementarity between their DNA functionalities. *Note that these experiments evidenced that PVP-capped g-AgNPs with a minimum of DNA conjugation could not migrate in the gel due to a lack of highly charged surface. Therefore, gel-based isolation of discrete NP assemblies (e.g. dimers) is not possible.*

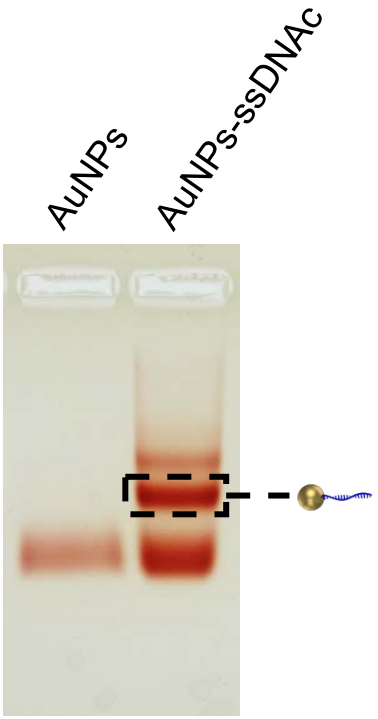

Figure S10-2. Agarose gel electrophoretic isolation of ssDNAc mono-functionalized 5 nm AuNPs. Lanes 1 and 2 correspond to 5 nm AuNPs before and after DNA conjugation. The DNA:AuNP molar ratio was 0.7:1 to ensure a maximized yield of the DNA-monoconjugated product.

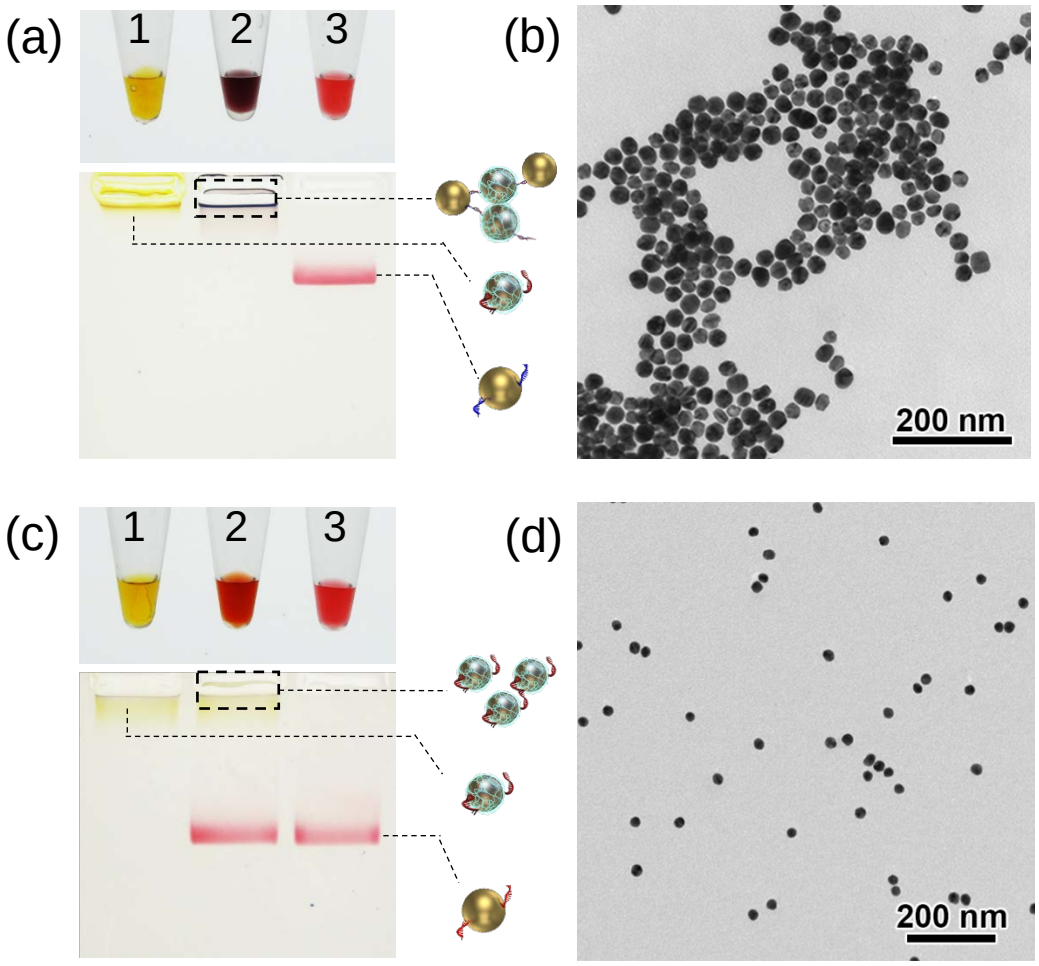

Figure S11. (a, b) Agarose gel electrophoretic analysis (a) and a TEM image (b) showing DNA-directed self-assembly between ssDNA-functionalized, PVP-protected g-AgNPs (lane 1) and ssDNAc-functionalized BSPP-capped AuNPs (lane 3). Lane 2 corresponds to self-assembled products as evidenced in (b). (c, d) Agarose gel electrophoretic (c) and TEM data (b) showing a control experiment where the same DNA (ssDNAc) was employed to functionalize PVP-protected g-AgNPs (sample 1) and BSPP-capped AuNPs (sample 3). The mixture between these two samples did not reveal any self-assembled products, as evidenced by the yellowish "product" (characteristic of g-AgNPs) in the gel well of lane 2 as well as a large excess of free AuNPs running into the gel. This result was further verified by TEM imaging (d).

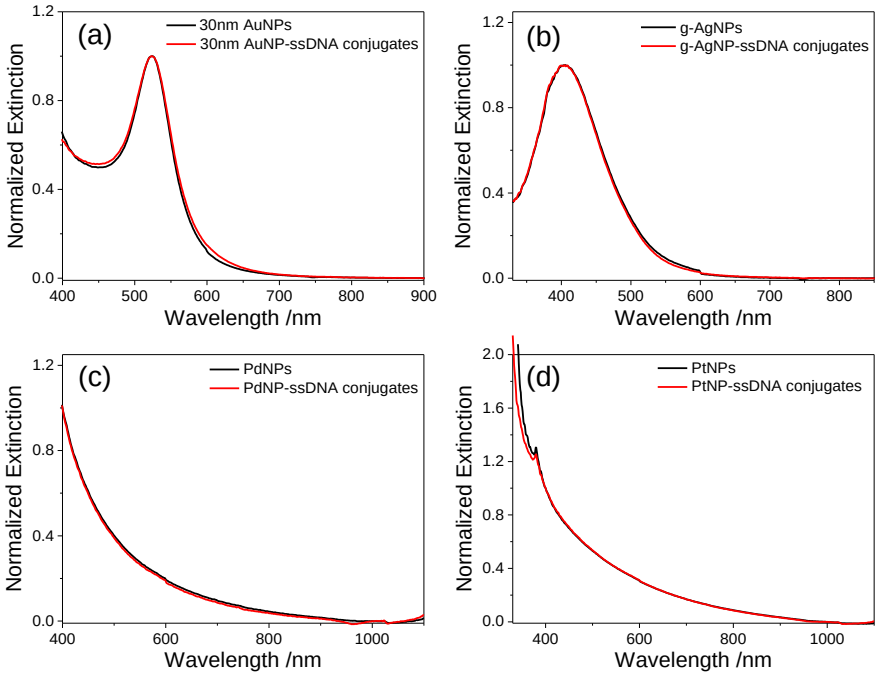

Figure S12. Extinction spectra of (a) AuNPs, (b) g-AgNPs, (c) PdNPs, and (d) PtNPs before and after DNA functionalization.

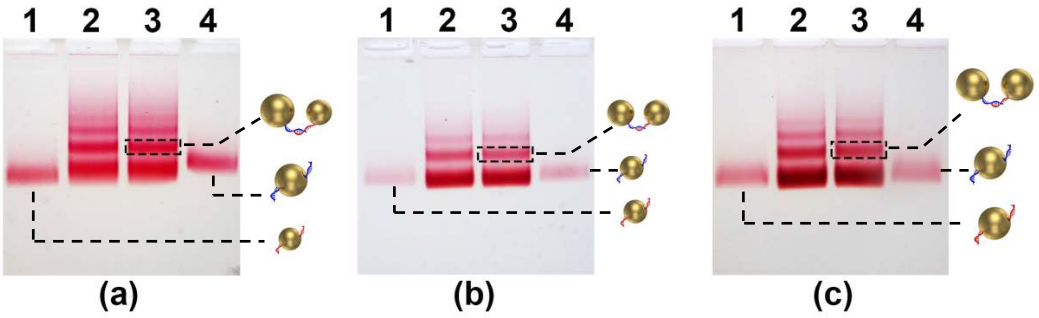

Figure S13. Agarose gel electrophoretic separations of DNA-assembled heterogeneous (a) and homogeneous (b, c) nanodimers composed of 23 and/or 30 nm AuNPs. Lanes 1 and 4 correspond to AuNPs minimally functionalized by ssDNA and ssDNAc strands, respectively. Lanes 2 and 3 are duplicates of the same DNA-directed AuNP assemblies from the monomers in lanes 1 and 4. In (b) and (c), the gel bands in lanes 2 and 3 correspond to monomers, dimers, trimers, and tetramers, etc. as counted from the bottom bands to the top ones. The products in (a) are somehow complicated due to the heterogeneous nanoparticle compositions. However, the dimer product can be easily assigned without ambiguity. The bands marked by rectangular boxes are dimeric products that can be extracted from the gels.

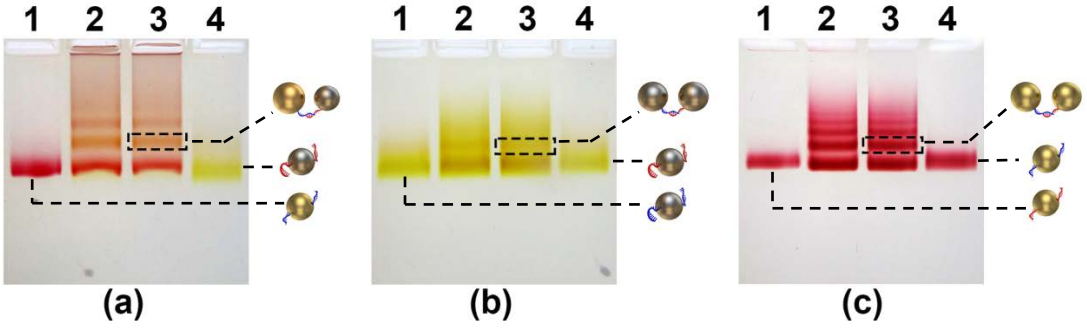

Figure S14. Agarose gel electrophoretic separations of DNA-assembled heterogeneous (a) and homogeneous (b, c) nanodimers composed of 30 nm AuNPs and/or g-AgNPs. Lanes 1 and 4 correspond to AuNPs/g-AgNPs minimally functionalized by ssDNA and ssDNAc, respectively. Lanes 2 and 3 are duplicates of the same DNA-directed AuNP/g-AgNPs assemblies from the monomers in lanes 1 and 4. In (b) and (c), the gel bands in lanes 2 and 3 correspond to monomers, dimers, trimers, and tetramers, etc. as counted from the bottom bands to the top ones. The products in (a) are somehow complicated due to the heterogeneous nanoparticle compositions. However, the dimer product can be easily assigned without ambiguity. The bands marked by rectangular boxes are dimeric products that can be extracted from the gels.

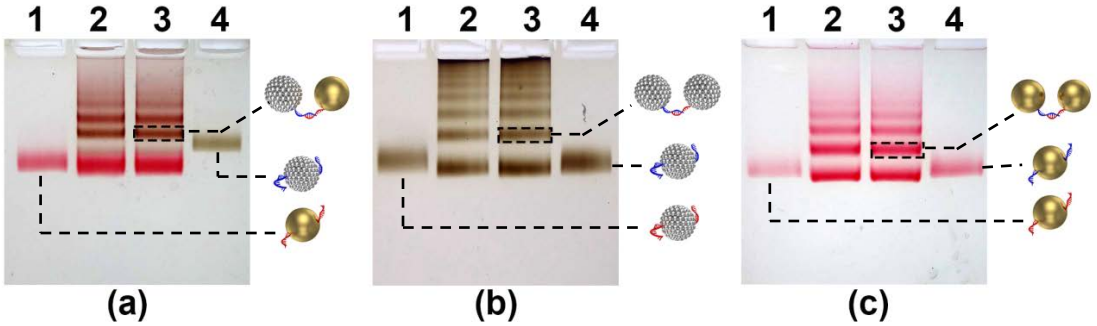

Figure S15. Agarose gel electrophoretic separations of DNA-assembled heterogeneous (a) and homogeneous (b, c) nanodimers composed of 30 nm AuNPs and/or 37 nm PtNPs. Lanes 1 and 4 correspond to AuNPs or PtNPs minimally functionalized by ssDNA and ssDNAc strands, respectively. Lanes 2 and 3 are duplicates of the same DNA-directed AuNP/PtNPs assemblies from the monomers in lanes 1 and 4. In (b) and (c), the gel bands in lanes 2 and 3 correspond to monomers, dimers, trimers, and tetramers, etc. as counted from the bottom bands to the top ones. The products in (a) are somehow complicated due to the heterogeneous nanoparticle compositions. However, the dimer product can be assigned without ambiguity. The bands marked by rectangular boxes are dimeric products that can be extracted from the gels.

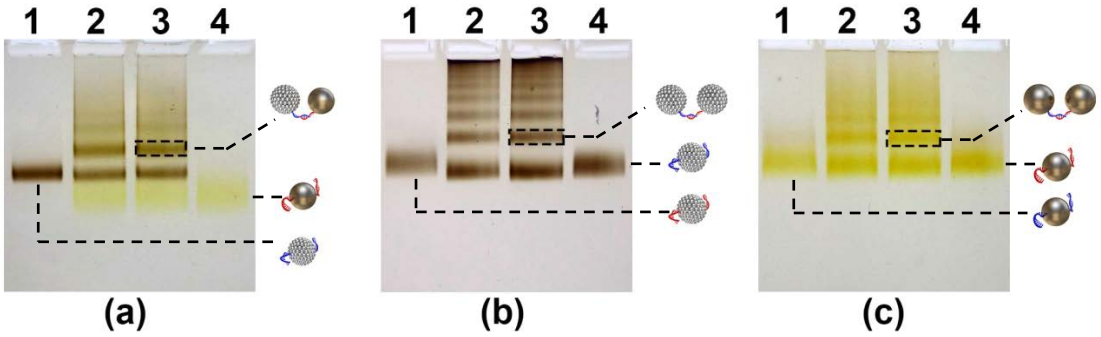

Figure S16. Agarose gel electrophoretic separations of DNA-assembled heterogeneous (a) and homogeneous (b, c) nanodimers composed of g-AgNPs and/or PtNPs. Lanes 1 and 4 correspond to g-AgNPs or PtNPs minimally functionalized by ssDNA and ssDNAc strands, respectively. Lanes 2 and 3 are duplicates of the same DNA-directed g-AgNPs/PtNPs assemblies from the monomers in lanes 1 and 4. In (b) and (c), the gel bands in lanes 2 and 3 correspond to monomers, dimers, trimers, and tetramers, etc. as counted from the bottom bands to the top ones. The products in (a) are somehow complicated due to the heterogeneous nanoparticle compositions. However, the dimer product can be easily assigned without ambiguity. The bands marked by rectangular boxes are dimeric products that can be extracted from the gels.

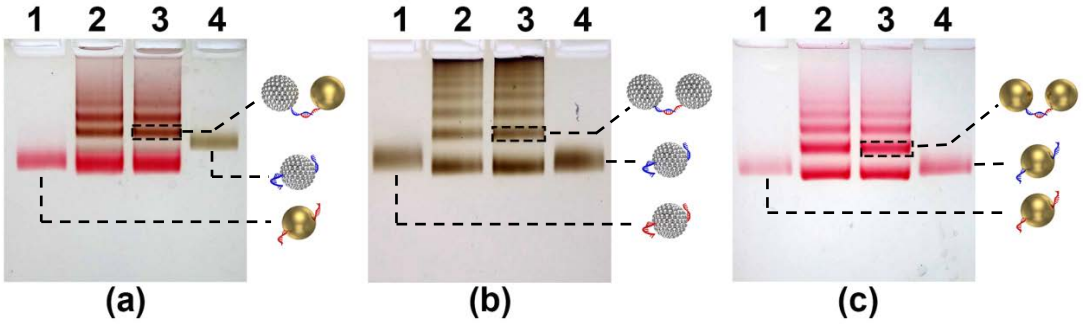

Figure S17. Agarose gel electrophoretic separations of DNA-assembled heterogeneous (a) and homogeneous (b, c) nanodimers composed of 30 nm AuNPs and/or 48 nm PdNPs. Lanes 1 and 4 correspond to AuNPs or PdNPs minimally functionalized by ssDNA and ssDNAc strands, respectively. Lanes 2 and 3 are duplicates of the same DNA-directed AuNP/PdNPs assemblies from the monomers in lanes 1 and 4. In (b) and (c), the gel bands in lanes 2 and 3 correspond to monomers, dimers, trimers, and tetramers, etc. as counted from the bottom bands to the top ones. The products in (a) are somehow complicated due to the heterogeneous nanoparticle compositions. However, the dimer product can be assigned without ambiguity. The bands marked by rectangular boxes are dimeric products that can be extracted from the gels.

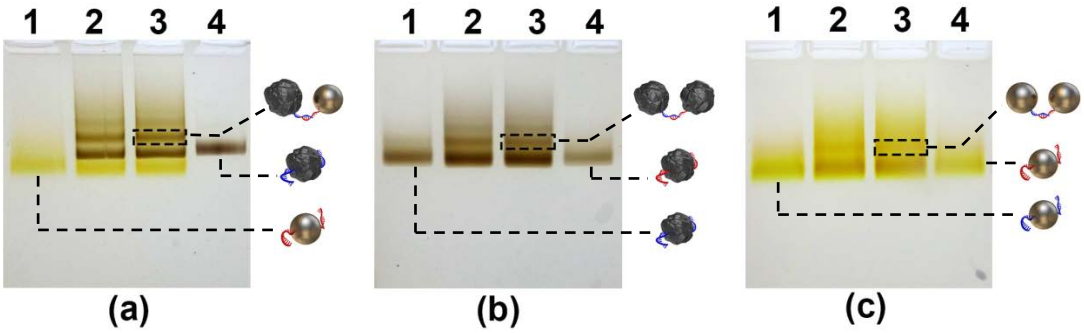

Figure S18. Agarose gel electrophoretic separations of DNA-assembled heterogeneous (a) and homogeneous (b, c) nanodimers composed of g-AgNPs and/or PdNPs. Lanes 1 and 4 correspond to g-AgNPs or PdNPs minimally functionalized by ssDNA and ssDNAc strands, respectively. Lanes 2 and 3 are duplicates of the same DNA-directed g-AgNPs/PdNPs assemblies from the monomers in lanes 1 and 4. In (b) and (c), the gel bands in lanes 2 and 3 correspond to monomers, dimers, trimers, and tetramers, etc. as counted from the bottom bands to the top ones. However, the products in (a) are somehow complicated due to the heterogeneous nanoparticle compositions. However, the dimer product can be assigned without any ambiguity. The bands marked by rectangular boxes are dimeric products that can be extracted from the gels.

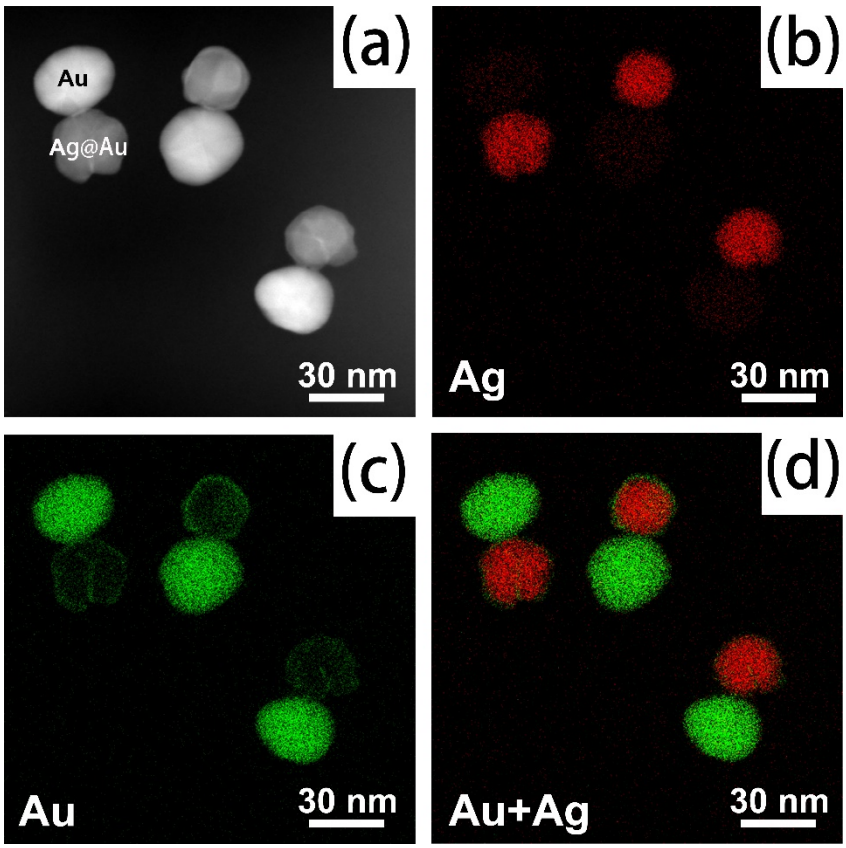

Figure S19. (a) High-angle annular dark-field scanning transmission electron microscopy (HAADF-STEM) imaging of AuNP/g-AgNP heterodimers. (b, c) Energy-dispersive X-ray spectroscopy (EDS) mapping of Ag (b) and Au (c) elements for the heterodimers shown in (a). (d) A merged image of (b) and (c).

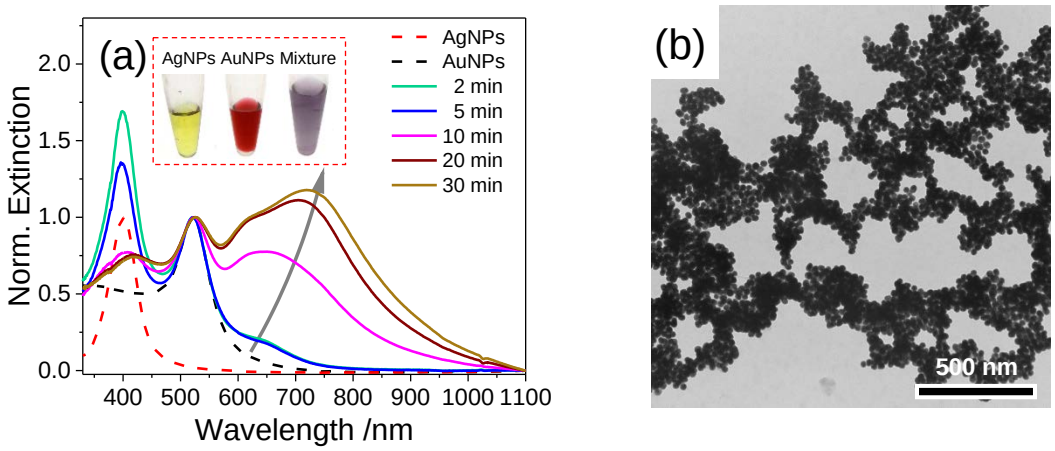

Figure S20. Oxidative silver leaching leads to aggregation of AuNPs in an Au/AgNPs mixture due to an Ag^+-soldering effect. (a) Extinction spectra and optical photos of samples; (b) TEM imaging of Au/AgNP aggregates after a 30-min mixing. *These data reveal an inherent difficulty in AuNP/AgNP heteroassembly.*

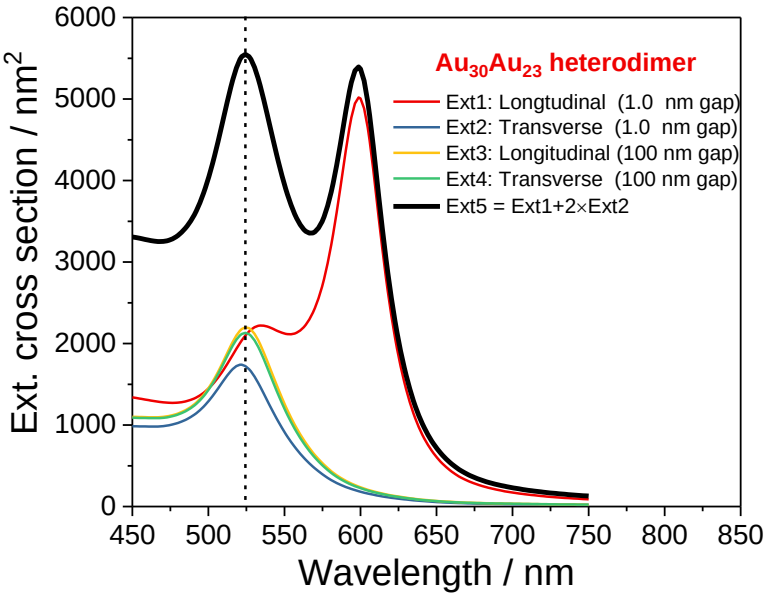

Figure S21: Simulated extinction spectra for an $Au_{30}Au_{23}$ heterodimer. Ext1 and Ext2 are longitudinal and transverse resonances for a dimer with a 1.0 nm gap. Ext3 and Ext4 are longitudinal and transverse resonances for a dimer with a 100 nm gap, which are equivalent to those of individual (uncoupled) AuNPs. The thick black line (Ext5) is an averaged spectrum of Ext1 and Ext2 considering transverse mode has a two-time chance to appear relative to the longitudinal mode for a random orientation. Therefore, Ext5 reasonably approximates the extinction spectrum of a randomly oriented dimer in solution. Accordingly, as indicated by a vertical dashed line in the figure, the shorter-wavelength peak in a coupled dimer (thick black line, 1.0 nm gap) is composed of a transverse plasmon mode (blue line) and some high order mode (red line). Anti-bonding longitudinal mode might also exist here. For an uncoupled dimer (100 nm gap), a peak located at the marked position comes from the extinctions of individual particles.

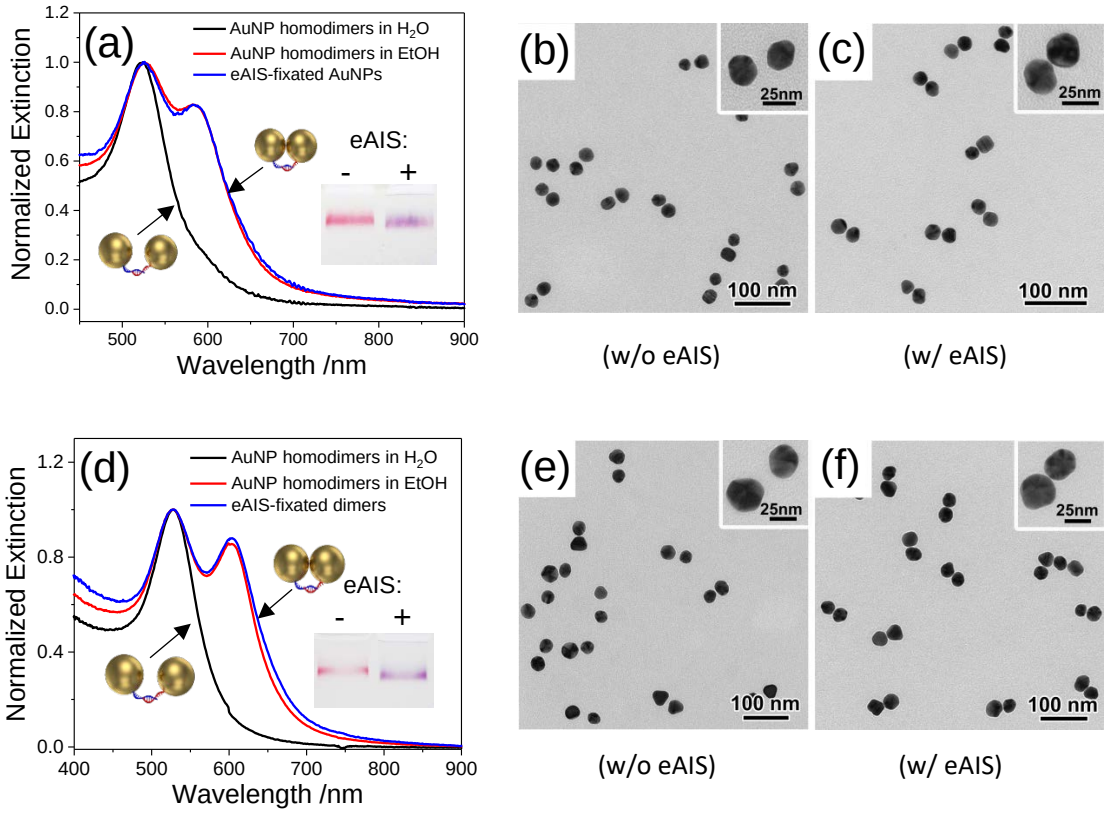

Figure S22. Optical extinction spectra and TEM images of DNA-assembled 23 nm (a-c) and 30 nm (d-f) AuNP homodimers with and without an eAIS treatment. The insets in (a) and (d) are agarose gel electropherograms of corresponding homodimers before and after eAIS fixation.

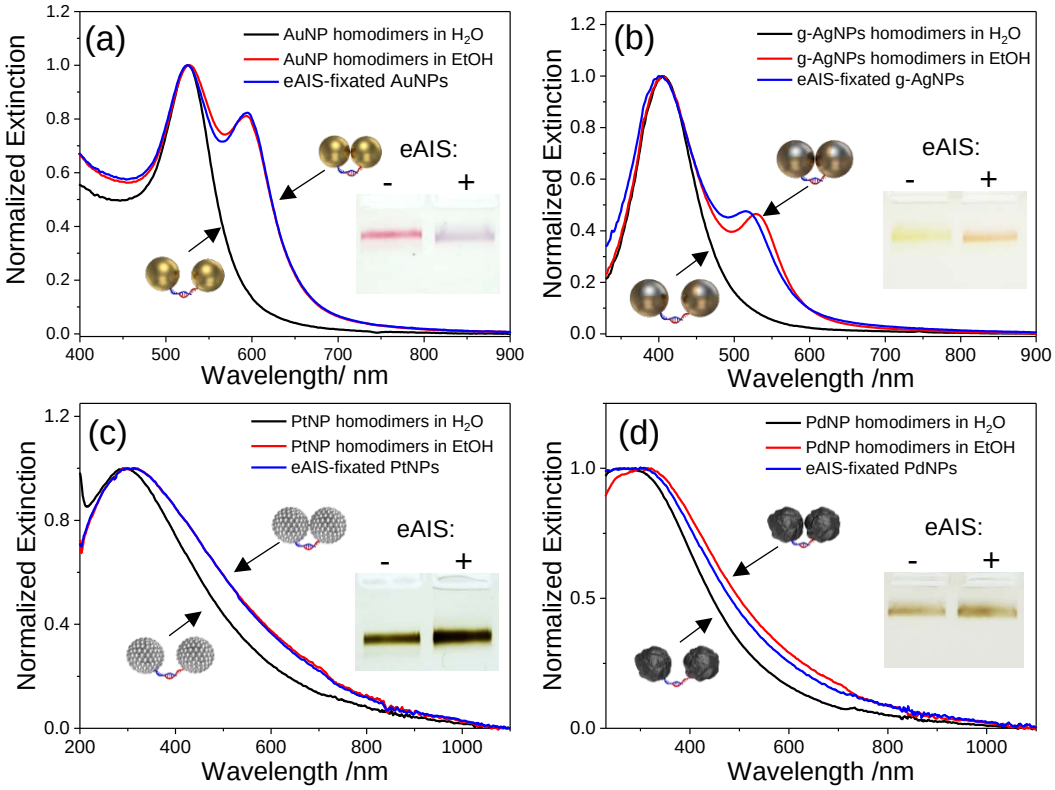

Figure S23. Optical extinction spectra of DNA-assembled homodimers of (a) 30 nm AuNPs, (b) 30 nm g-AgNPs, (c) 48 nm PtNPs, and (d) 37 nm PdNPs before and after an eAIS treatment. The insets are agarose gel electropherograms of the corresponding structures.

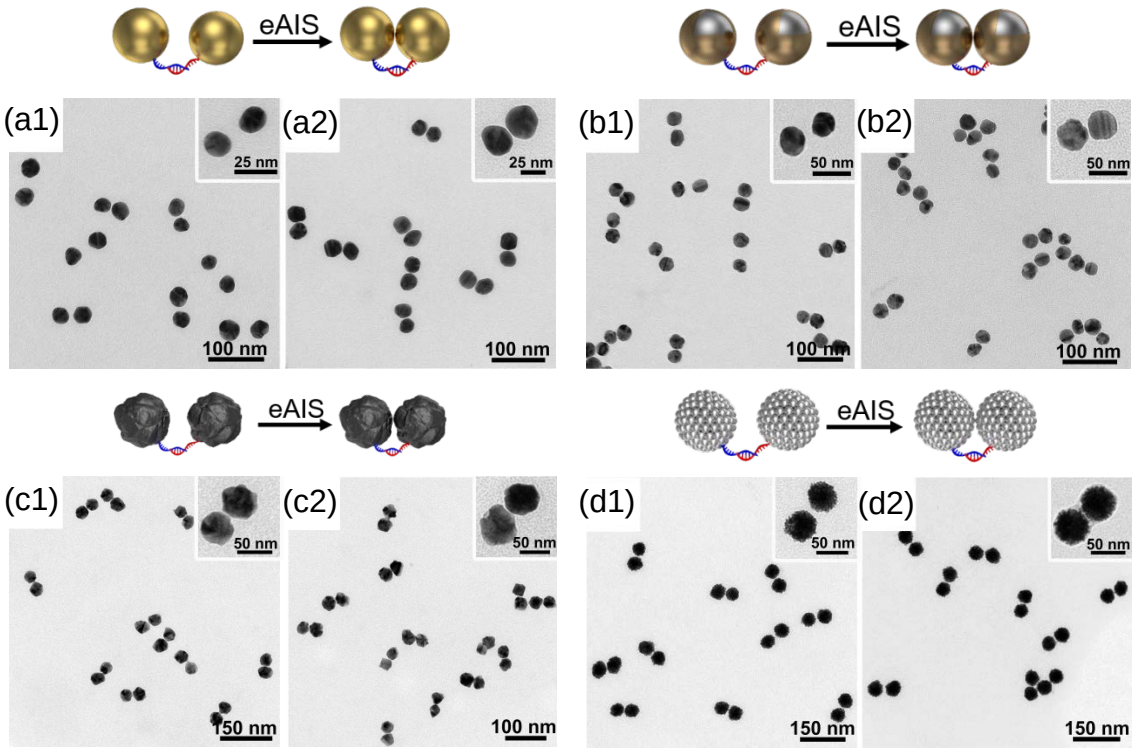

Figure S24. TEM of DNA-assembled homodimers of (a, b) 30 nm AuNPs, (c, d) 30 nm g-AgNPs, (e, f) 48 nm PtNPs, and (g, h) 37 nm PdNPs before (a1, b1, c1, d1) and after (a2, b2, c2, d2) eAIS treatments. *Due to intra-dimeric capillary dragging forces during TEM sample preparations, dimers of relatively large particles appeared closely associated under TEM which did not reflect their well-separated configurations in native buffer solutions.*

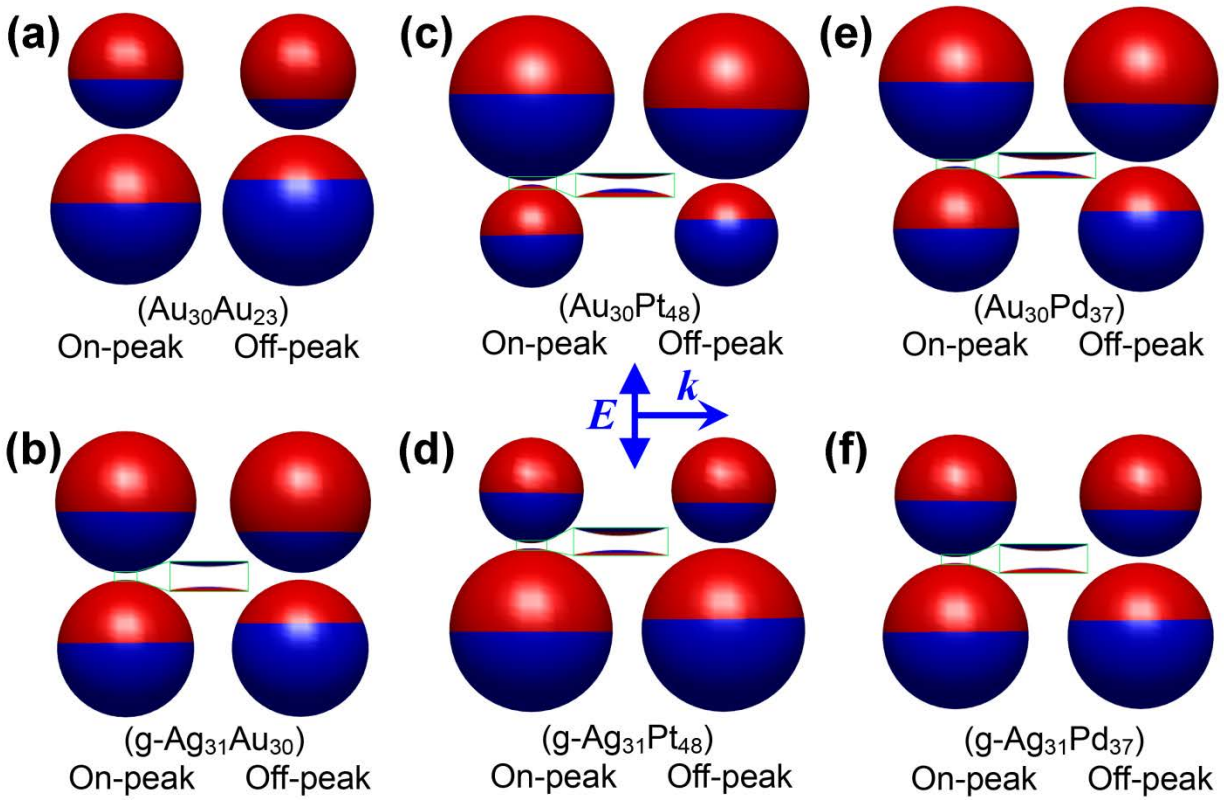

Figure S25. BEM-calculated auxiliary outer-surface charge distributions of different heterodimers with excitation wavelengths of incident planar waves fixed at the extinction peaks ("on-peak") as well as the half-maximum positions at the red-edges of the extinction peaks. Gap sizes were set to be 1.0 nm for upper panels, and 1.5 nm for lower panels. Such red-shifted excitations result in a purely dipolar feature of the resulting plasmon resonances as judged from the charge distributions, which is clearly different from the on-peak excitations where slight convolutions from higher-order quadrupole coupling are visible (see insets of zoomed gap regions).

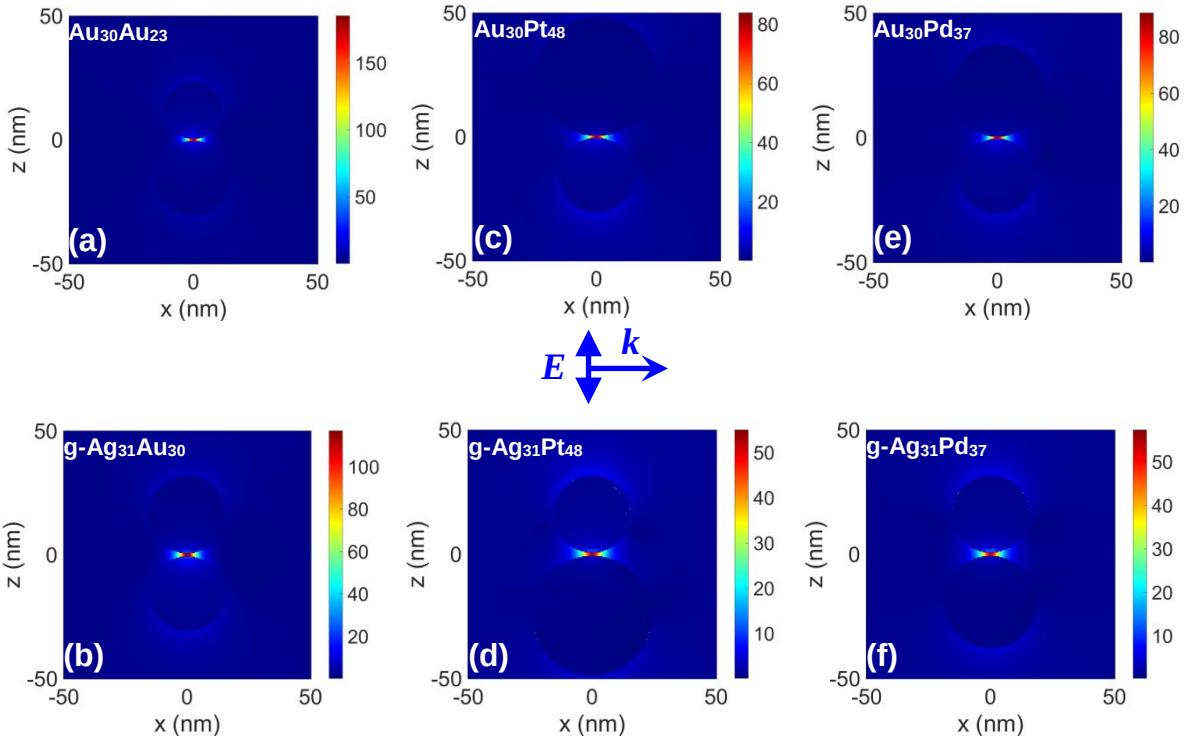

Figure S26. BEM-calculated e-field distributions of different heterodimers excited at the half-maximum positions on the red-edges of the extinction peaks (off-peak) in Figure 4 (gap sizes set to be 1.0 nm for upper panels, and 1.5 nm for lower panels). Panels (a-f) correspond to the dimer structures (a-f) in Figure S24.

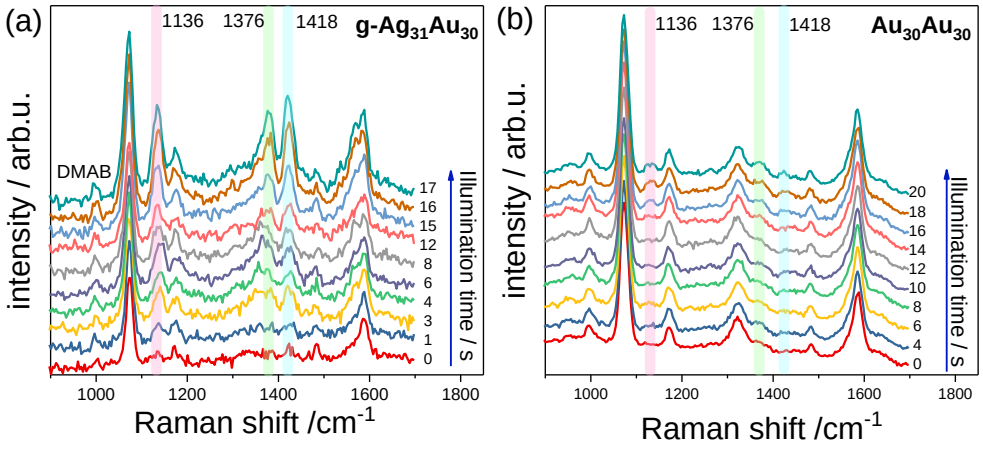

Figure S27. Plasmon-medicated photocatalytic oxidization of para-aminothiophenol (p-ATP) into *p,p'*-dimercaptoazobenzene (DMAB) in the hotspots of the dimers under the irradiation of a 633 nm Raman laser. Au-Ag heterodimers (a) showed a better catalytic activity than Au-Au homodimers (b) probably due to their different surface activity. Characteristic vibrations (1136, 1376, and 1418 cm^{-1}) of the DMAB product are marked on the spectra. These data revealed the chemical addressability of the nanogaps, and demonstrated their potential applications in surface enhanced Raman scattering (SERS) and plasmonic catalysis.

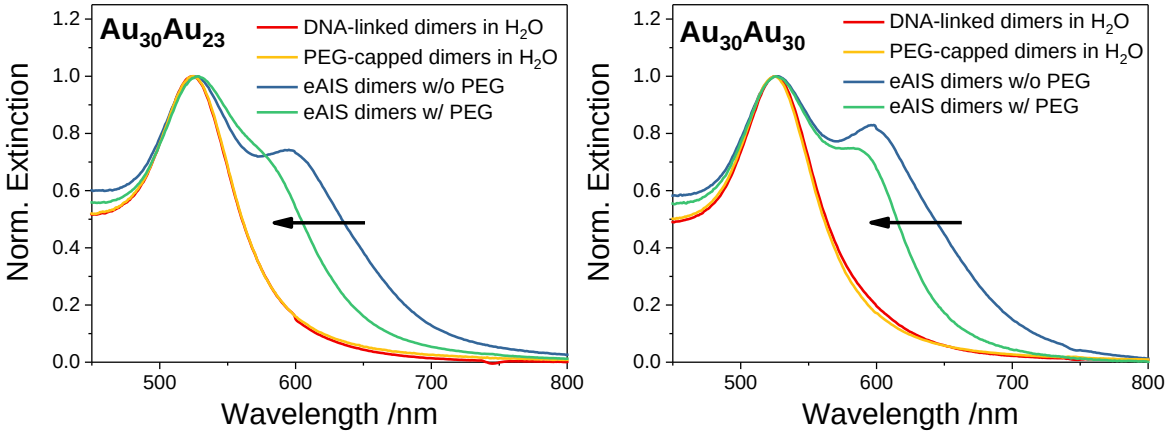

Figure S28. Extinction spectra showing the tuning of gap-dependent BDP resonances for $Au_{30}Au_{23}$ heterodimers and $Au_{30}Au_{30}$ homodimers. These data demonstrated that the PEG ($HS\text{-}PEG_8\text{-}COOH$) capping layer significantly increased the gap size of the eAIS-coupled dimers such that blue-shifted longitudinal peaks were observed for both hetero- and homo-dimers. PEG:AuNP molar ratio was 1000:1.

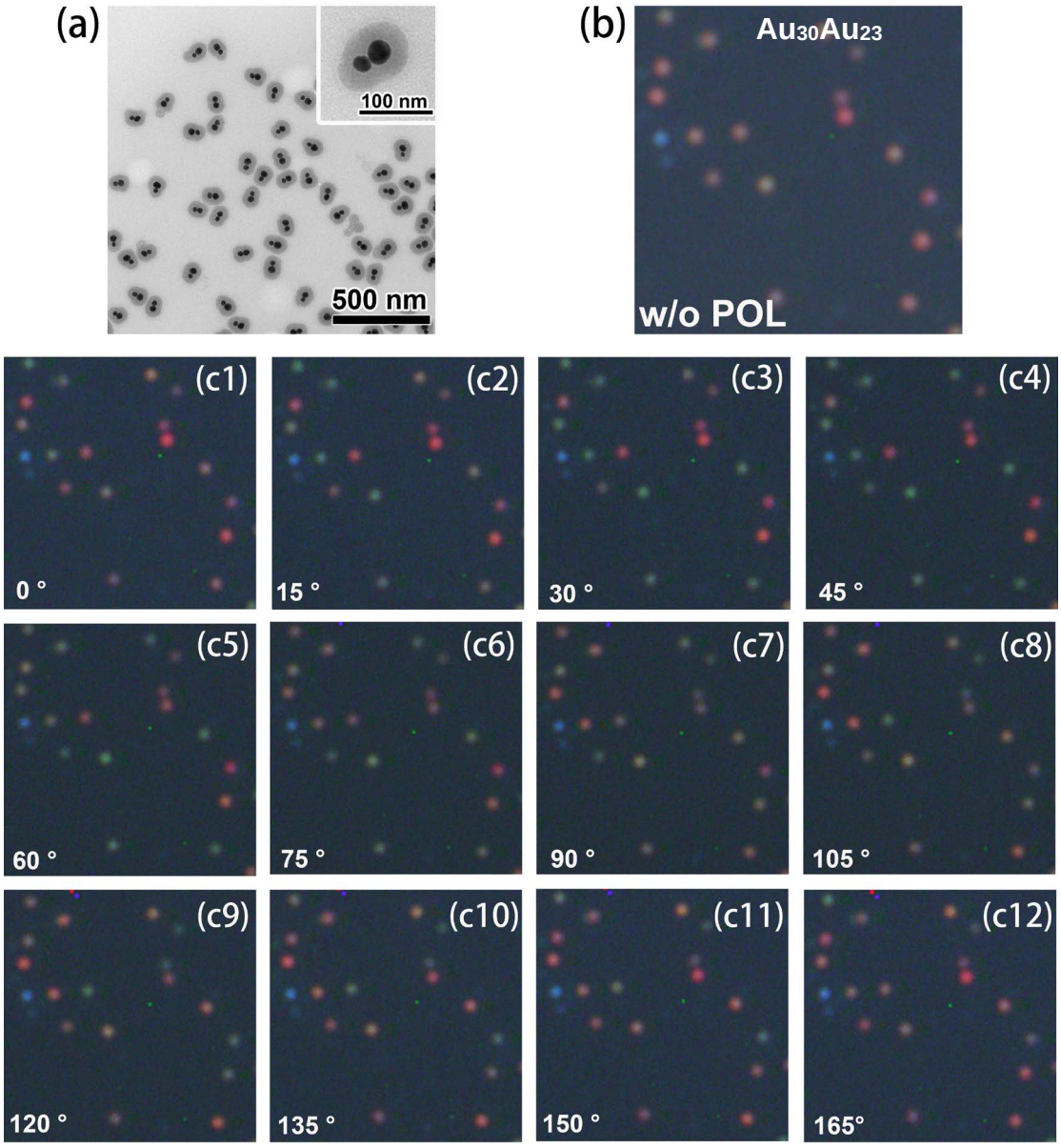

Figure S29. Dark field imaging of silica-encapsulated, strongly coupled $Au_{30}Au_{23}$ heterodimers with or without a polarization control of incident light. TEM imaging (a) verified the high purity of as-prepared dimers. A dark field image in (b) (in the absence of a polarizer) indicated that most of the dimer particles were strongly coupled due to their characteristic colors deviated from individual particles that scatter pure green light. A change of polarization angle caused periodical color changes of most of the particles between green and red/purple colors, verifying their orientation-dependent longitudinal and transverse plasmon resonances. The silica shells guaranteed a correct judgement of the dimeric coupling by avoiding interdimeric plasmon interactions in possibly occurred aggregates in the surface-deposited samples. The images were contrast-enhanced due to the weak scattering intensities of the relatively small particles (CCD noises are visible from the pictures). Some blue particles on the images were defects on the glass slide, which did not come from AuNPs.

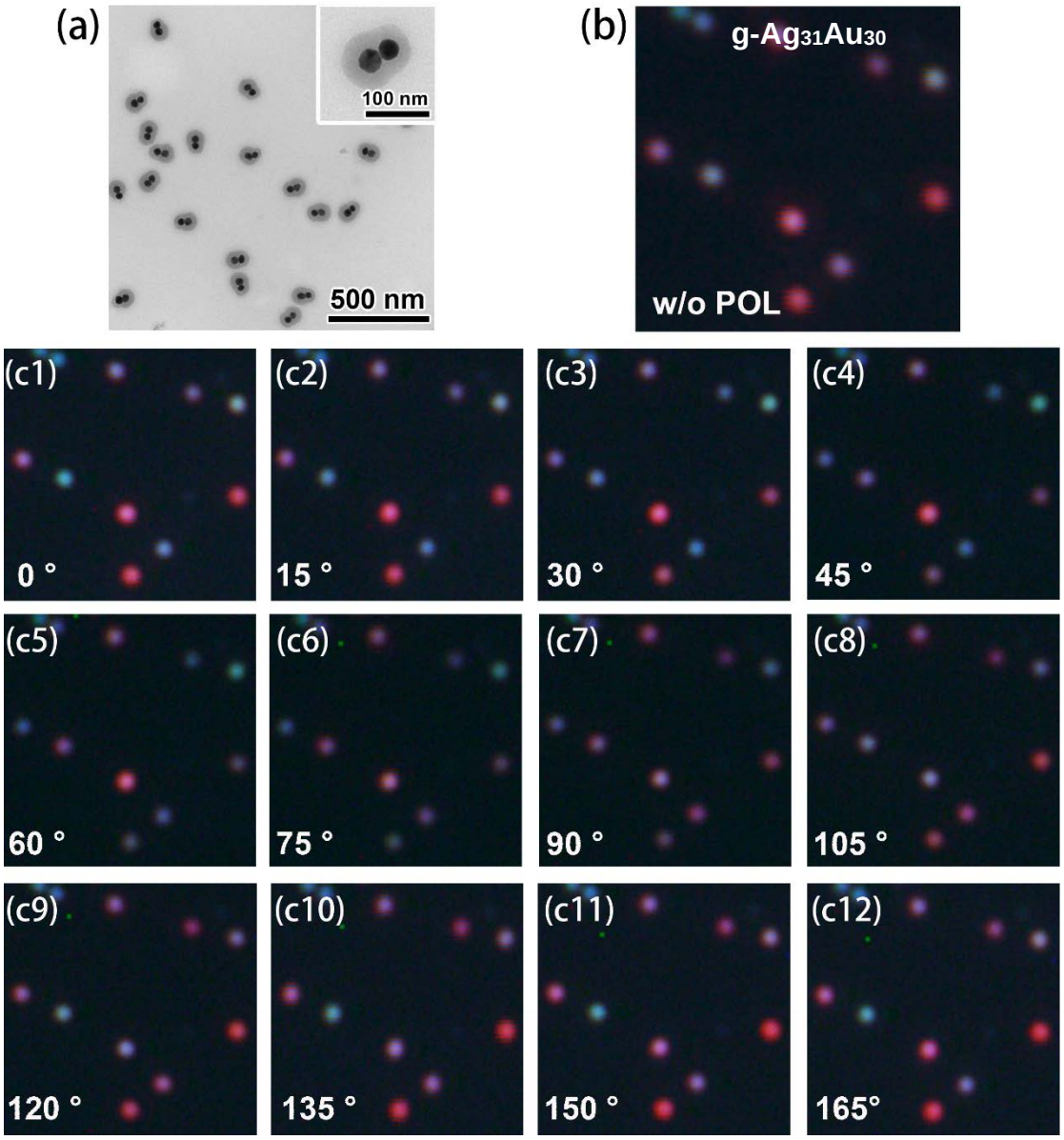

Figure S30. Dark field imaging of silica-encapsulated, strongly coupled g-$Ag_{31}Au_{30}$ heterodimers with or without a polarization control of incident light. TEM imaging (a) verified the high purity of as-prepared dimers. A dark field image in (b) (in the absence of a polarizer) indicated that most of the dimer particles were strongly coupled due to their characteristic colors deviated from individual particles that scatter pure blue (Ag) or green (Au) light. A change of polarization angle caused periodical color changes of most of the particles between cyan and purple colors (in this case, rich colors existed for the dimers due to the compositionally asymmetric feature of the structures), verifying their orientation-dependent longitudinal and transverse plasmon resonances. The silica shells guaranteed a correct judgement of the dimeric coupling by avoiding interdimeric plasmon interactions in possibly occurred aggregates in the surface-deposited samples. The images were contrast-enhanced due to the weak scattering intensities of the relatively small particles (CCD noises are visible from the pictures).

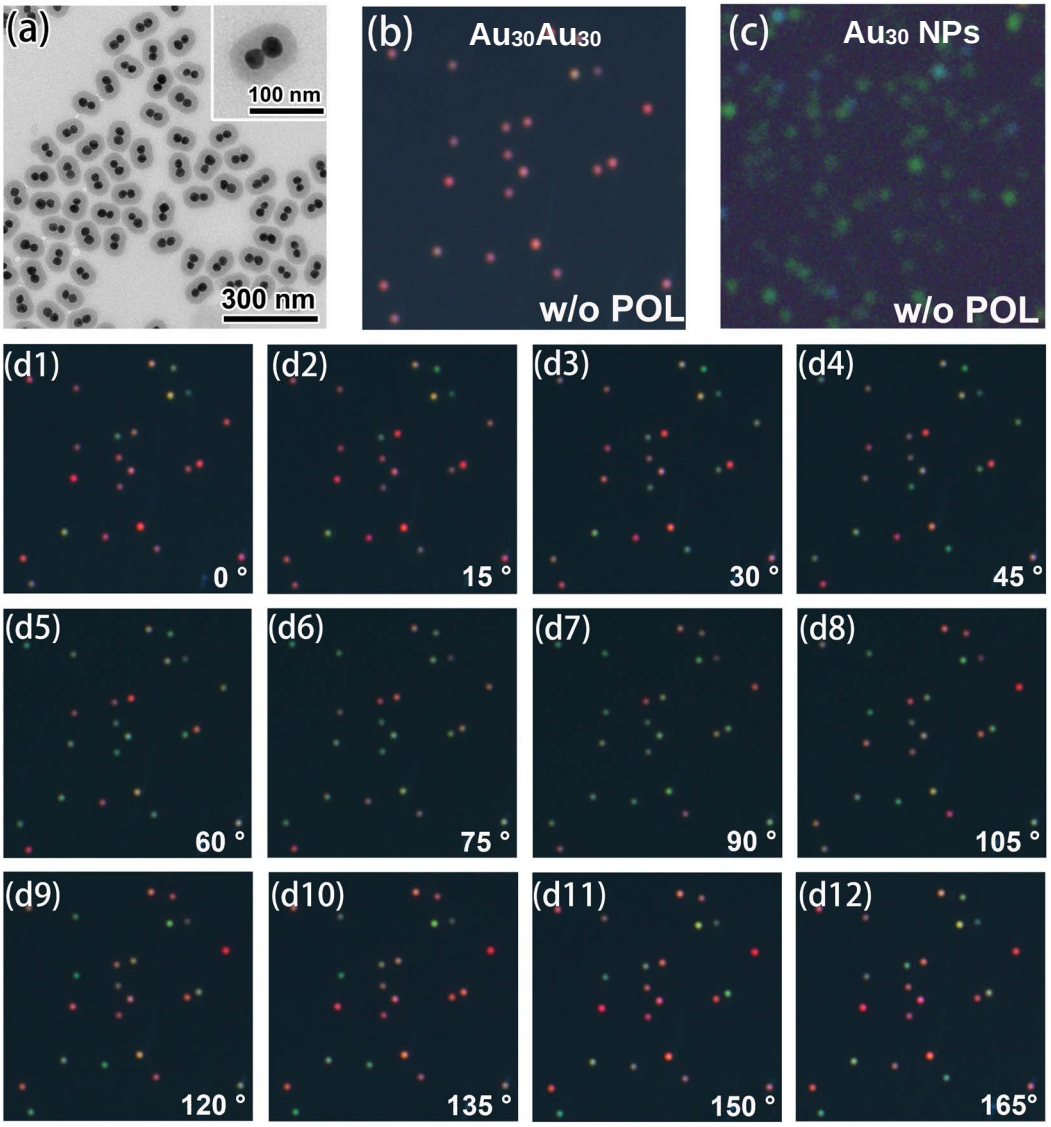

Figure S31. Dark field imaging of silica-encapsulated, strongly coupled $Au_{30}Au_{30}$ homodimers with or without a polarization control of incident light. TEM imaging (a) verified the high purity of as-prepared dimers. A dark field image in (b) (in the absence of a polarizer) indicated that most of the dimer particles were strongly coupled due to their characteristic colors deviated from individual particles that scattered pure green light (c). A change of polarization angle caused periodical color changes of most of the particles between green and red/purple colors, verifying their orientation-dependent longitudinal and transverse plasmon resonances. The silica shells guaranteed a correct judgement of the dimeric coupling by avoiding interdimeric plasmon interactions in possibly occurred aggregates in the surface-deposited samples. The images were contrast-enhanced due to the weak scattering intensities of the relatively small particles (CCD noises are visible from the pictures).

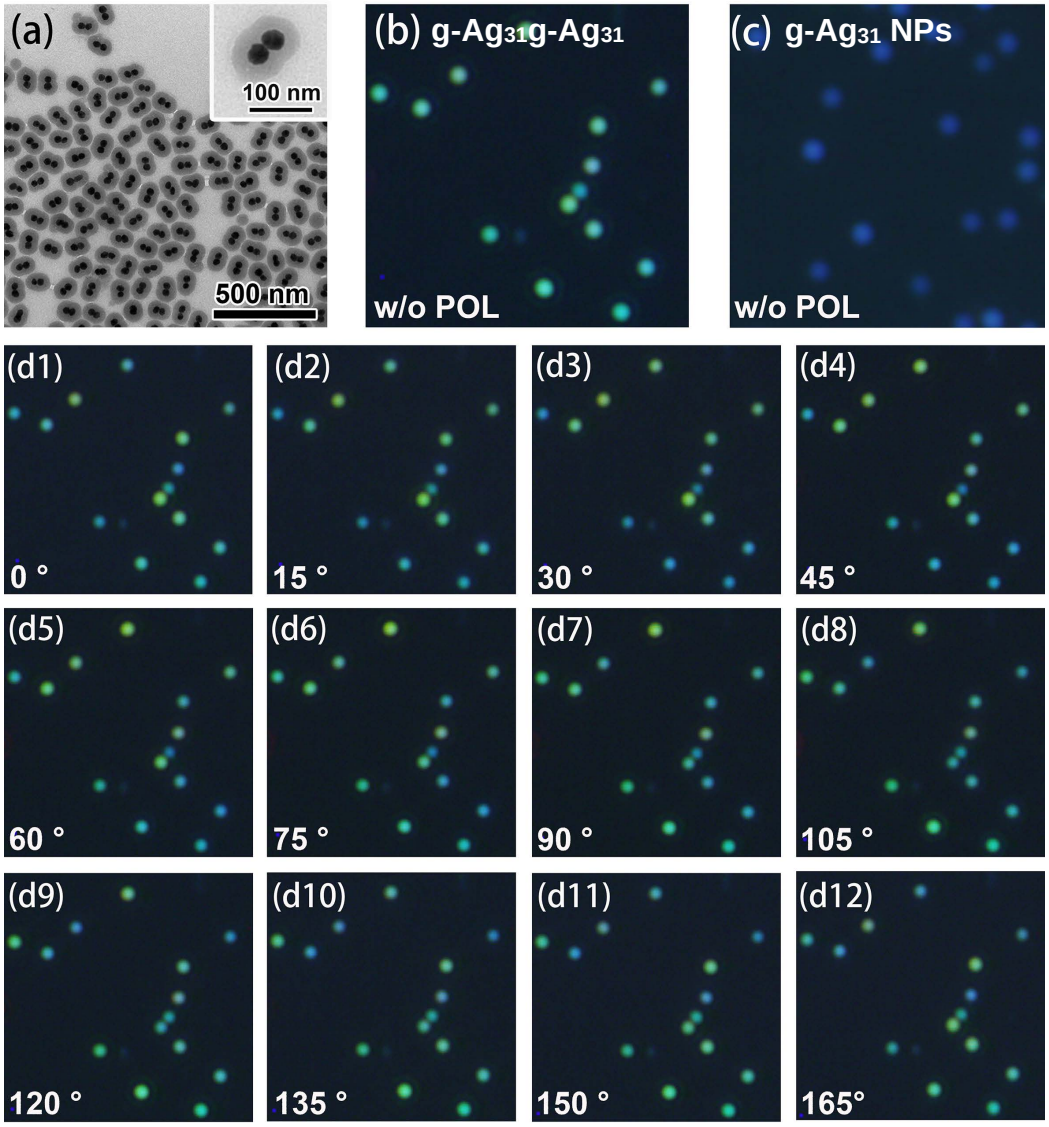

Figure S32. Dark field imaging of silica-encapsulated, strongly coupled g-Ag_{31}g-Ag_{31} homodimers with or without a polarization control of incident light. TEM imaging (a) verified the high purity of as-prepared dimers. A dark field image in (b) (in the absence of a polarizer) indicated that most of the dimer particles were strongly coupled due to their characteristic colors deviated from individual particles that scattered pure blue light (c). A change of polarization angle caused periodical color changes of most of the particles between blue and cyan/green colors, verifying their orientation-dependent longitudinal and transverse plasmon resonances. The silica shells guaranteed a correct judgement of the dimeric coupling by avoiding interdimeric plasmon interactions in possibly occurred aggregates in the surface-deposited samples. The images were contrast-enhanced due to the weak scattering intensities of the relatively small particles (CCD noises are visible from the pictures).

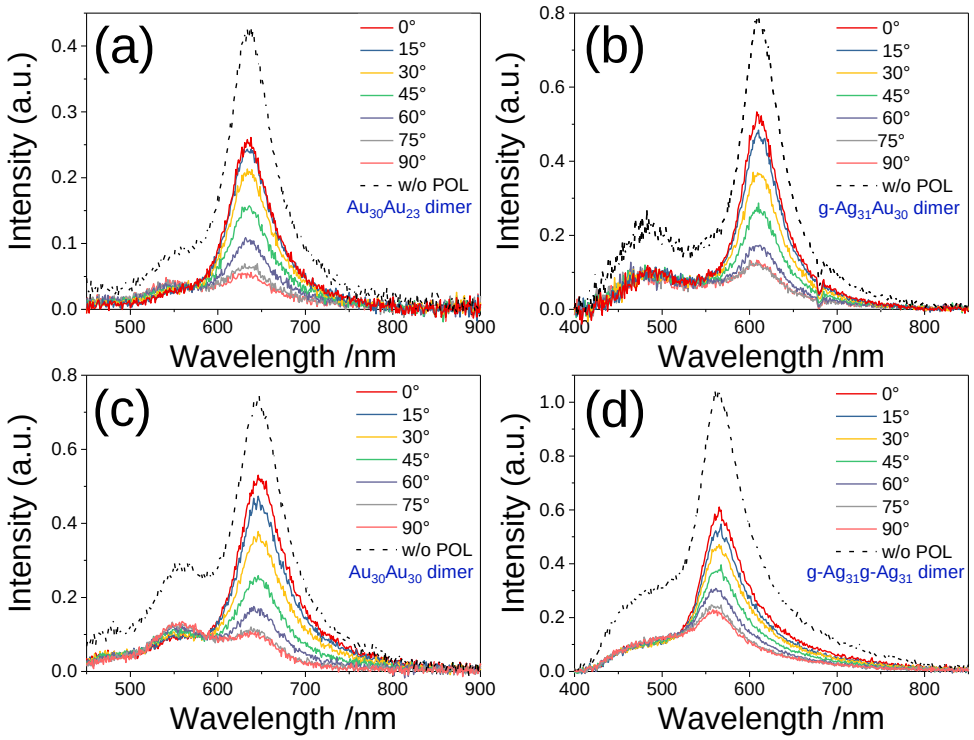

Figure S33. Dark-field scattering spectra collected from a single structure of $Au_{30}Au_{23}$ heterodimer (a), g-$Ag_{31}Au_{30}$ heterodimer (b), $Au_{30}Au_{30}$ homodimer (c), and g-Ag_{31}g-Ag_{31} homodimer (d) as a function of polarization angle (0-90°). Dashed lines are spectra recorded without a polarizer. The polarization-dependent spectra were consistent with the anisotropic dimeric structures. 0° and 90° correspond to longitudinal and transverse orientations of the dimers, respectively. Some residual longitudinal signals at a 90° polarization angle probably came from some nonidealities of the optical setup and improper orientations of dimers. Bonding transverse modes of asymmetric dimers should also appear around this position. Drifting of the samples during a relatively long time recording of the weak signals also caused some instability of the measurement. The spectra were background corrected, and normalized by an intensity distribution of the incident light source.